DOCKET NO: 220523US0PCT

IN THE UNITED STATES PATENT & TRADEMARK OFFICE

IN RE APPLICATION OF	:
MAKOTO YONEYA, ET AL.	: EXAMINER: NGUYEN, HOAN C.
SERIAL NO: 10/070,908	:
FILED: JULY 12, 2002	: GROUP ART UNIT: 2871
FOR: LIQUID CRYSTAL DISPLAY DEVICE	:

APPEAL BRIEF UNDER 37 C.F.R. § 41.37

COMMISSIONER FOR PATENTS
ALEXANDRIA, VIRGINIA 22313

SIR:

Further to the Final Office Action of October 20, 2006 and the Advisory Action of May 15, 2007, Applicants request review of the rejections of the above-identified application by the Board of Patent Appeals and Interferences.

(I) REAL PARTY IN INTEREST

The real party in interest is Japan Science and Technology Corporation.

(II) RELATED APPEALS AND INTERFERENCES

None.

(III) STATUS OF THE CLAIMS

Claims 1-22 are pending in the application. Claims 2, 8-20 and 22 are presently withdrawn from consideration. Claims 1, 3-7 and 21 are rejected claims. The rejection of Claims 1, 3-7 and 21 is appealed.

(IV) STATUS OF THE AMENDMENTS

The arguments and/or amendment of the submissions of January 22, 2007; July 31, 2006; February 13, 2006; September 16, 2005; July 12, 2005; November 8, 2004; and the Preliminary Amendment submitted on July 12, 2002 were entered and considered. A Pre-Appeal Brief Request for Review submitted on September 16, 2006 was considered.

(V) SUMMARY OF THE CLAIMED SUBJECT MATTER

Independent Claim 1 is drawn to a liquid crystal display device. The display device includes a pair of substrates at least one of which is transparent. The substrates are identified as SUB1 and SUB2 in Figure 2 of the specification. A nematic liquid crystal layer is present between the pair of substrates. The nematic liquid crystal layer is identified as LCL in Figure 2. The liquid crystal display device includes a group of interdigitated electrodes formed on at least one of the substrates. Figure 2 identifies the electrodes as EL1B and EL2A. An alignment layer is present between the nematic liquid crystal layer and at least one of the substrates (see the layer identified as AL1 in Figure 2). The alignment layer is one that has been subjected to liquid crystal anchoring treatments in more than one direction (see the paragraph bridging pages 5 and 6 of the specification). The pre-tilt angle of the liquid crystal molecules in the anchoring direction with respect to the substrate surface is substantially zero (see the sentence bridging pages 5 and 6, the last paragraph on page 6 and FIG. 1(b)). The

interdigitated electrodes form an electric field component that is substantially parallel to the surfaces of the substrates (see for example page 17, lines 11-17).

(VI) GROUNDS OF REJECTION

Claims 1, 3-7 and 21 are rejected as anticipated under the meaning 35 U.S.C. § 102(b) over a patent to Kim (U.S. 6,091,471). The Office asserts that Kim discloses all of the limitations of present Claim 1 (see pages 3 and 4 of the October 20, 2006 Office Action). In particular, the Office asserts that liquid crystal displays having an in-plane switching mode inherently have interdigitated electrodes (see page 2 of the Advisory Action of March 15, 2007). The Office asserts that Kim discloses a nematic liquid crystal cell having in-plane switching mode (see page 2 of the Office Action of October 20, 2006). The Office asserts that an alignment layer having a pre-tilt layer of substantially 0° obtained by a rubbing treatment is disclosed in Figure 14 of Kim (see page 2 of the October 20, 2006 Office Action).

(VII) ARGUMENT

A) The Office's assertion that liquid crystal cells having an in-plane switching mode inherently have interdigitated electrodes is factually not correct and ignores Applicants' factual evidence. The rejection of the present claims as anticipated over Kim is not supportable and should be withdrawn because Kim does not disclose all of the present claims limitations; namely the office has not shown that Kim discloses a device having interdigitated electrodes..

The claimed liquid crystal display must have interdigitated electrodes (see line 4 of Claim 1 of Appendix VIII). One basis for the Office's rejection of the present claims as anticipated is the Office's assertion that liquid crystal cells having an in-plane switching

mode inherently have interdigitated electrodes. Applicants submitted technical publications authored by Clark ("Sub-Microsecond Bistable Electro-Optic Switching in Liquid Crystals"); Patel ("Flexoelectric Electro-Optics of a Cholesteric Liquid Crystal"), and Jaegemalm ("An Electro-Optic Device Based on Field-Controlled Anchoring of a Nematic Liquid Crystal") as evidence that liquid crystal cells having an in-plane switching mode do not inherently have interdigitated electrodes (see attachments of Appendix IX).

On pages 2-3 of the Amendment filed on July 31, 2006 and pages 5-8 of the Amendment filed on January 22, 2007, Applicants pointed out that the liquid crystal display devices of Clark, Patel and Jaegemalm do not have interdigitated electrodes. In particular, the Request for Reconsideration filed on January 22, 2007 gave reasons why Clark discloses a liquid crystal cell having an in-plane switching mode but does not have interdigitated electrodes (see page 7, line 7 to page 8, line 3 of the January 22 Request for Reconsideration). The reason why Jaegemalm discloses a liquid crystal display device having an in-plane switching mode without requiring interdigitated electrodes was argued on page 5, line 24 through page 7, line 22 of the January 22, 2007 Request for Reconsideration. The reason why Patel discloses a liquid crystal display device having an in-plane switching mode and not having interdigitated electrodes was discussed on page 6, line 18 through page 7, line 6 of the January 22, 2007 Request for Reconsideration.

The Offices responded to Applicants' factual data and arguments by asserting that Tomioka (U.S. 6,682,783) discloses a liquid crystal display device having interdigitated electrodes. Applicants point out that Tomioka does not disclose that all liquid crystal display devices having an in-plane switching mode necessarily have interdigitated electrodes. As pointed out by Applicants on page 5, lines 1-20 of the January 22 Request for Reconsideration, at best, Tomioka provides a general statement of the background art but does not disclose that all liquid crystal display devices having an in-plane switching mode

necessarily have interdigitated electrodes. Thus, the evidence contradicts the Office's assertion that liquid crystal display devices having an in-plane switching inherently have interdigitated electrodes

In the Advisory Action of March 15, 2007, the Office responded to Applicants' arguments that liquid crystal display devices having an in-plane switching mode do not inherently have interdigitated electrodes by citing additional portions of Tomioka and further by citing to Held (U.S. 6,177,972) and Broer (U.S. 7,123,319). See page 2 of the Advisory Action of March 15. With respect to the Office's reliance on Tomioka and Held, Applicants point out that the information cited by the Office is insufficient to demonstrate that liquid crystal display devices having an in-plane switching mode inherently, i.e., in all cases, have interdigitated electrodes. At best, Tomioka and Held disclose particular liquid crystal display devices that may, e.g., optionally, have interdigitated electrodes. Tomioka and Held do not disclose that all liquid crystal display devices having an in-plane switching mode have interdigitated electrodes.

With respect to the Office's reliance on Broer, Applicants point out that Broer is not prior art to the present application. The Office's reliance on Broer in support of the rejections is legally not correct. Moreover, the Office stated that interdigitated electrodes are "comb-shaped" but provided no support for this statement (see the first sentence on page 2 of the March 15 Advisory Action).

In a contradictory statement, the Office conceded in the last sentence on page 2 of the March 15 Advisory Action that Clark, Patel and Jaegemalm do not in fact disclose interdigitated electrodes:

> All references, Clark, Patel and Jaegemalm do not disclose the interdigitated electrodes, which inherently generate the electric field parallel to the substatrates as the applicants' invention.

To the extent the Office's rejection can be understood, Applicants submit that the Office's assertion that liquid crystal display devices having an in-plane switching mode inherently have interdigitated electrodes is factually incorrect as evidenced by the Office's own statement in the last sentence of the March 15, 2006 Advisory Action and further in view of Applicants' factual evidence including the technical publications of Clark, Patel and Jaegemalm.

Applicants have provided ample evidence that prior art liquid crystal display devices having an in-plane switching do not have interdigitated electrodes. The rejection of the present claims as anticipated is thus unsupportable and should be withdrawn.

B). The Office's assertion that the prior art relied on by the Office discloses a liquid crystal display device having a layer with a pre-tilt angle of substantially 0° is factually not correct. The rejection of the present claims as anticipated over Kim is not supportable and should be withdrawn at least because Kim does not disclose all of the present claims limitations.

In support of the rejection the Office cited to Figure 14 and/or 4 of Kim (see page 3 of the Office Action of May 18, 2005). Applicants traversed the rejection in the Request for Reconsideration filed on February 13, 2006 (see pages 9-10).

The prior art alignment layer is prepared by a rubbing treatment. On July 12, 2005, Applicants submitted evidence that a rubbing treatment cannot provide a pre-tilt angle of substantially 0°. The purpose of providing this evidence was to traverse the Office's assertion that the Figures of Kim disclose an alignment layer having a pre-tilt angle of substantially 0°. Applicants argued in the Request for Reconsideration filed on July 12, 2005 that the alignment layer of Kim is obtained by treating a layer by rubbing (see page 8, line 4 – page 10, line 22 July 12, 2005 Request for Reconsideration).

Each of the technical attachments submitted in traversal of the rejection, i.e., Geary (*J. Appl. Phys.*, pp. 4100-4108) and Seo (*Jpn. J. Appl. Phys.*, pp. L503-L506) discloses that a rubbing treatment, such as the rubbing treatment used in Kim to align the prior art layer, cannot provide an alignment layer having a pre-tilt angle of substantially zero (see also pages 2, line 7 – page, 4, line 15 of the Pre-Appeal Brief filed on September 16, 2005).

The Office failed to respond to Applicants' arguments in any meaningful way in this regard. Even though the January 22, 2007 Request for Reconsideration pointed out that the Office did not respond to this argument (see page 2 of the January 22, 2007 Request for Reconsideration), the Advisory Action of March 15, 2007 did not respond to Applicants' argument and factual evidence.

Applicants submit that the rejection of the present claims on the grounds that Kim discloses an alignment layer having a pre-tilt angle of substantially 0° is not supportable at least because Applicants submitted evidence showing that a rubbing treatment cannot provide an alignment layer having a pre-tilt angle of substantially 0°. Applicants further submit the rejection is not appropriate in view of the fact that the Office has not substantively considered and/or responded to Applicants' arguments in this regard in any meaningful way.

The January 22, 2007 Request for Reconsideration further argued that Kim does not disclose an alignment layer having pre-tilt angles of substantially 0° as evidenced by Kim's use of one-headed arrows to indicate the direction of alignment. Applicants argued at length in the response filed on July 31, 2006 that the use of a one-headed arrow in the Figures of Kim show that the prior art pre-tilt angle is not substantially 0° (see page 3, line 22 – page 5, line 20 of the July 31, 2006 Amendment). Applicants referenced publications authored by Seo and Lien as evidence showing that a two-headed arrow indicates a pre-tilt angle of substantially 0° but a one-headed arrow does not (see page 4, line 5 from the bottom to page 5, line 6 from the bottom of the July 31 response).

As discussed above for the argument that Kim does not disclose a pre-tilt angle having substantially 0° because a mechanical rubbing treatment cannot provide such a pre-tilt angle, the Office appears to have completely ignored Applicants' arguments that Kim does not disclose the alignment layer of the present claims on the basis that Kim uses a one-headed arrow which necessarily cannot represent a pre-tilt angle of substantially 0°.

In summary, the Office failed to consider and respond to all of Applicants' arguments and evidence submitted in support of patentability. The Office's rejection is based on a factually incorrect assertions regarding the presence of interdigitated electrodes in prior art devices and the pre-tilt angle of certain layers of the prior art devices. The Office's response consistently ignores Applicants' arguments and mischaracterizes the evidence.

The rejections should be withdrawn in view of the Office's factual errors and refusal to consider Applicants' arguments in support of patentability.

Respectfully submitted,

OBLON, SPIVAK, McCLELLAND,
MAIER & NEUSTADT, P.C.
Norman F. Oblon

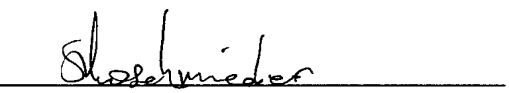

Stefan U. Koschmieder, Ph.D.
Registration No. 50,238

Customer Number
22850

Tel: (703) 413-3000
Fax: (703) 413 -2220
(OSMMN 03/06)

VIII. CLAIMS APPENDIX

Claim 1: A liquid crystal display device comprising

a pair of substrates, at least one of which is transparent;

a nematic liquid crystal layer between the pair of substrates;

a group of interdigitated electrodes formed on at least one of the substrates and adapted to apply an electric field to said liquid crystal layer, wherein the electric field has a component substantially parallel to the surfaces of the substrates;

and an alignment layer disposed between the nematic liquid crystal layer and at least one of the substrates,

wherein the alignment layer has been subjected to liquid crystal anchoring treatments in plural directions to form a plurality of liquid crystal in-plane anchoring directions,

the plurality of liquid crystal in-plane anchoring directions of the alignment layer form substantially equal angles relative to one another on the corresponding substrate surface,

a pretilt angle in each of the liquid crystal anchoring directions with respect to the corresponding substrate surface is substantially zero.

Claim 2: A liquid crystal display device comprising

a pair of substrates, at least one of which is transparent;

a liquid crystal layer between the pair of substrates;

a group of electrodes formed on at least one of the substrates and adapted to apply an electric field to the liquid crystal layer, the electric field having component substantially parallel to the surfaces of the substrates; and

an alignment layer disposed between the liquid crystal layer and at least one of the substrates

wherein the alignment layer has been subjected to liquid crystal anchoring treatments in two directions to form two liquid crystal in-plane anchoring directions;

the two liquid crystal in-plane anchoring directions of the alignment layer form an angle of about 90° relative to each other on the corresponding substrate surface;

a pretilt angle in one liquid crystal anchoring direction with respect to the corresponding substrate surface is substantially zero,

a pretilt angle in the other liquid crystal anchoring direction with respect to the corresponding substrate surface is not substantially zero; and

the device is capable of maintaining two stable in-plane alignment states of the liquid crystal layer even after the removal of the applied electric field.

Claim 3: A liquid crystal display device according to claim 1, wherein at least one of the liquid crystal anchoring treatments in plural directions comprises

performing uniform anchoring treatment over an entire target area in each of the in-plane directions.

Claim 4: A liquid crystal display device according to claim 1, wherein at least one of the liquid crystal anchoring treatments in plural in-plane directions comprises

dividing an entire target area into plural sub-areas corresponding to the plural in-plane directions and

performing anchoring treatment in each of the sub-areas in the corresponding in-plane direction.

Claim 5: A liquid crystal display device according to claim 1, wherein at least one of the liquid crystal anchoring treatments in plural in-plane directions comprises

irradiating the alignment layer with linearly polarized light which is capable of causing a chemical reaction on the surface of the corresponding substrate.

Claim 6: A liquid crystal display device according to claim 1, wherein at least one of the liquid crystal anchoring treatments in plural in-plane directions comprises

scanning the alignment layer with a probe which is capable of imparting stress to the surface of the corresponding substrate.

Claim 7: A liquid crystal display device according to claim 1, wherein at least one of the liquid crystal anchoring treatments in plural in-plane directions comprises

scanning the alignment layer with light which is capable of causing a chemical reaction on the surface of the corresponding substrate.

Claim 8: A liquid crystal display device according to claim 1, wherein the liquid crystal layer comprises a liquid crystal material which comprises chiral molecules.

Claim 9: A liquid crystal display device according to claim 1, wherein the liquid crystal layer comprises a liquid crystal material having a positive or negative dielectric anisotropy depending on the frequency of an applied AC electric field.

Claim 10: A liquid crystal display device according to claim 1, further comprising an additional electrode on each of the substrates wherein the additional electrodes form a pair.

Claim 11: A liquid crystal display device according to claim 1, further comprising a light reflection plate on one of the substrates.

Claim 12: A liquid crystal display device according to claim 2, wherein at least one of the liquid crystal anchoring treatments in plural in-plane directions comprises

performing uniform anchoring treatment over an entire target area in each of the in-plane directions.

Claim 13: A liquid crystal display device according to claim 2, wherein at least one of the liquid crystal anchoring treatments in plural in-plane directions comprises

dividing an entire target area into plural sub-areas corresponding to the plural in-plane directions and

performing anchoring treatment in each of the sub-areas in the corresponding in-plane direction.

Claim 14: A liquid crystal display device according to claim 2, wherein at least one of the liquid crystal anchoring treatments in plural in-plane directions comprises

irradiating the alignment layer with linearly polarized light which is capable of causing a chemical reaction on the surface of the corresponding substrate.

Claim 15: A liquid crystal display device according to claim 2, wherein at least one of the liquid crystal anchoring treatments in plural in-plane directions comprises

scanning the alignment layer with a probe which is capable of imparting stress to the surface of the corresponding substrate.

Claim 16: A liquid crystal display device according to claim 2, wherein at least one of the liquid crystal anchoring treatments in plural in-plane directions comprises

scanning the alignment layer with light which is capable of causing a chemical reaction on the surface of the corresponding substrate.

Claim 17: A liquid crystal display device according to claim 2, wherein the liquid crystal layer comprises a liquid crystal material which comprises chiral molecules.

Claim 18: A liquid crystal display device according to claim 2, wherein the liquid crystal layer comprises a liquid crystal material having a positive or negative dielectric anisotropy depending on the frequency of an applied AC electric field.

Claim 19: A liquid crystal display device according to claim 2, further comprising an additional electrode on each of the substrates wherein the additional electrodes form a pair.

Claim 20: A liquid crystal display device according to claim 2, further comprising a light reflection plate on one of the substrates.

Claim 21: The liquid crystal display device according to claim 1, wherein the device is capable of maintaining a plurality of stable in-plane alignment states of the liquid crystal layer even after the removal of the applied electric field.

Claim 22: The liquid crystal display device according to claim 2, wherein the in-plane alignment states remain energetically stable even after removal of applied voltage.

IX. EVIDENCE APPENDIX

The evidence submitted by Applicants, including publications by Patel, Clark, Jaegemalm, Seo, Geary and Lien were previously submitted to the Office during prosecution. Copies of the aforementioned publications are attached.

The mechanism of polymer alignment of liquid-crystal materials

J. M. Geary, J. W. Goodby, A. R. Kmetz, and J. S. Patel
AT&T Bell Laboratories, Murray Hill, New Jersey 07974

(Received 30 December 1986; accepted for publication 27 July 1987)

Smetic and nematic liquid-crystal materials can be homogeneously aligned by buffed thin films of appropriate polymers. We propose that the buffing process orients the polymer's molecular chains in a manner similar to cold drawing of bulk polymer samples. Experimental verification of this theory is obtained by measuring buffing-induced birefringence in thin films of various polymers coated on glass. Further experiments establish that the oriented state of the polymer chains, and not scratching or grooving of the surface, is necessary to produce alignment. Alignment is found to occur when the polymer is both oriented and crystalline. A picture of alignment is presented in which the formation of a liquid-crystal phase on the crystalline,oriented polymer surface is analogous to the epitaxial growth of conventional solid crystals.

I. INTRODUCTION

Homogeneous alignment of liquid-crystal materials can be achieved by coating the surfaces of the cell that is to contain the liquid crystal with a very thin film of a linear polymer which is mechanically rubbed or buffed.[1,2] In the case of nematic materials, this method provides alignment superior to the weak alignment that can be produced by buffing uncoated surfaces. The method also yields good alignment of smectic materials, which are otherwise very difficult to align by buffing.

It is of considerable practical and theoretical interest to understand the mechanism by which such polymer alignment methods work. Specifically what alteration of the polymer takes place when the surface is rubbed? How does this alteration act to align the liquid-crystal molecules? And, especially in the case of smectics, why do some polymers produce good alignment while others produce no alignment at all?

One possibility is that polymer alignment acts through grooves or scratches induced by the buffing process.[3,4] While such a mechanism may be applicable to some situations, we find it to be an unsuitable explanation in the case of buffed polymer alignment for two reasons. First, alignment can be produced by buffing with a soft material and using a light pressure, conditions that seem unlikely to produce substantial scratching of the polymer surface. Second, different polymers are observed to differ strikingly in their ability to align. Using electron microscopy, we have found that buffed polymer surfaces can exhibit strong aligning ability and yet show no evidence of scratching or grooving. Even if significant scratching were to occur during buffing, this cannot explain the variation in aligning ability, since we find that the variation is uncorrelated with the mechanical hardness of the polymer.

An alternative concept is that alignment acts through the orientation of polymer molecules. The hypothesis has been advanced by Castellano[5] that buffing can orient the molecular chains of a polymer coating through localized melting, producing an aligning surface. Others have reported experimental evidence implying that oriented polymer surfaces can act to align liquid-crystal materials. Kondo *et al.*[6] have described alignment of smectics close to cell spacers made from oriented polymer sheets. Aoyama *et al.*[7] have reported alignment of nematics in cells whose surfaces were made of stretched polymer films. Aligning ability of dip-coated polymer films along the direction of withdrawal from a polymer solution, without any buffing, has been reported by Becker *et al.*[8] More recently, Clark[9] observed surface memory effects on polymer-coated surfaces and attributed them to plastic deformation of the polymer film.

The present article is an experimental investigation of the hypothesis that polymer chain orientation can act to align liquid-crystal materials. There are two physical processes that must be considered: (1) the orientation of the polymer by the buffing process and (2) the interaction of the oriented polymer with the liquid-crystal material to cause alignment. Concerning the first process, a mechanism is proposed through which buffing can produce chain orientation in a thin polymer film in a manner resembling the cold drawing of a bulk polymer sample. The orientation of polymer chains by buffing is experimentally verified by birefringence measurements, and additional experiments are presented which support and clarify the mechanism. The second of the two physical processes is investigated by observing alignment caused by various polymers, both in conventional cells and in cells formed from cold-drawn bulk polymer samples. It is found that crystallinity of the polymer, as well as chain orientation, is necessary for the aligning effect to occur. Finally, an analogy is drawn between the epitaxial growth of conventional solid crystals and the formation of a liquid-crystal phase on the surface of a crystalline, oriented polymer surface.

II. THE BUFFING PROCESS

Buffing of the polymer-coated surface is accomplished by the undirectional motion of a fibrous material which is pressed into contact with the surface. The fibers of buffing materials are generally a number of micrometers in diameter, while the polymer films used in liquid-crystal alignment are typically 200–300 Å thick. The contact area between fiber and polymer that is created by the buffing pressure, while substantially less than the fiber diameter, can reasona-

 0021-8979/87/224100-09$02.40

bly be expected to be substantially broader than the film's thickness. Hence, during buffing the polymer film is caught between two broad planes, one stationary (the substrate) and the other moving (the fiber contact area). Thus, the polymer will experience a shearing force, and, if the friction exerted by the fiber contact area is great enough, a permanent shearing deformation can result.

The geometry of such a deformation is illustrated in cross section in Fig. 1. A rectangular portion of the film will tend to be sheared into a parallelogram [Fig. 1(b)], a form of deformation equivalent to pure elongation along the principal axes of stress oriented at 45°, as shown. With continued deformation, an extreme parallelogram form [Fig. 1(c)] will be produced. In this state, the axis of elongation, illustrated in the figure, will be nearly parallel to the polymer surface. Thus, through the action of shearing, the polymer film will be deformed much as if it had first been elongated by cold drawing and then placed upon the substrate. The deformed film will differ from this state only in that its axis of elongation will be somewhat inclined with respect to the substrate, to a degree dependent on the extent of deformation.

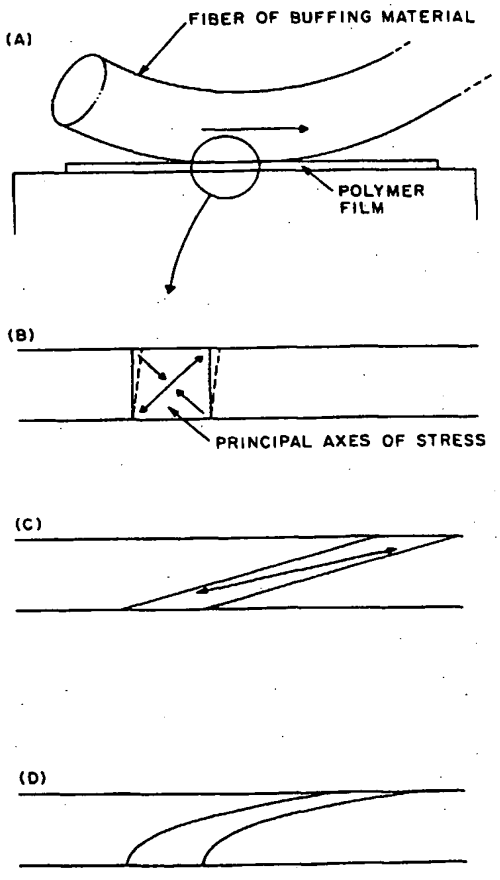

FIG. 1. (a) Cross-section view of a polymer film in contact with a moving fiber of buffing material. (b) Magnified view of the film under shearing forces, showing the principle axes of stress. (c) Effect of large shear deformation, similar to that which would be produced by simple elongation parallel to the substrate. (d) Modified version of large shear deformation, taking into account a possible proximity effect exerted by the substrate surface on the polymer.

The parallelogram form shown in Fig. 1(c) is of course an idealization. The plastic deformation of polymers is complex and may involve both nonlinear and hysteretic effects. This complexity is evident when the cold-drawing behavior of bulk polymer samples is examined. Often the sample "necks down" as it is stretched so that a thin, fully elongated segment is created somewhere along the length of the sample. This segment grows as regions of rapid plastic deformation advance into the undeformed portions of the sample. In polycrystalline samples, the degree of crystallinity increases as a result of the elongation, and the crystallites become oriented. Strongly amorphous polymers sometimes neck down also and can exhibit a directional correlation of their polymer chains while remaining noncrystalline. In the situation of Fig. 1, the deformation process is further complicated by the extreme thinness of the polymer film which makes it likely that surface effects will be significant. Binding of the polymer chains at points where they contact the substrate could lead to deformation like that suggested in Fig. 1(d). Experimental evidence presented in Sec. III C points to such a deformation profile as being more realistic than that of Fig. 1(c).

Whatever the precise form of the shearing deformation produced by the buffing process, there will always be a residual inclination of the elongation axis of the polymer at the surface. This inclination provides a natural explanation for the common observation in nematics that the direction of rub is reflected in a small tilt of the aligned liquid-crystal molecules. Such a "tilt bias" has always been difficult to understand from the viewpoint of a scratching or grooving mechanism of alignment. It is known that when the buffing material moves over the surface to the right, as shown in Fig. 1, the molecules of the liquid crystal will align so as to be tilted up slightly at their right-hand ends. This sense of tilt is the same as the sense of tilt of the orientation axis of the polymer in the figure. We feel that this correspondence between polymer orientation and liquid-crystal alignment with regard to both existence and sense of tilt tends to support the picture of buffing-induced deformation presented in Fig. 1. We will examine this point further in Sec. III D.

III. EXPERIMENTAL OBSERVATION OF POLYMER CHAIN ORIENTATION

In the above section, the hypothesis of buffing-induced polymer chain orientation has been described. In this section, experimental evidence supporting this hypothesis is presented. Polymer chain orientation is known to induce birefringence. This is a consequence of the difference in refractive index for light polarized parallel to and perpendicular to the polymer chains. Birefringence is induced both by crystalline orientation of the polymer chains and by noncrystalline directional correlation of the chains, as in the case of strongly amorphous polymers. We have employed measurement of birefringence to detect chain orientation that is induced by the buffing process. A number of different polymers were investigated in this manner, and it was found that the effects of buffing correspond in considerable detail to the effects of cold drawing of bulk polymers.

A. Apparatus

Birefringence was measured by means of the apparatus illustrated in Fig. 2. Light from a dc-powered incandescent source passed in sequence through a 633-nm narrow-band filter, a polarizer, a quarter-wave plate, the sample, and a crossed analyzer before reaching a silicon photodiode. The sample consisted of a piece of glass coated with a thin polymer film. During measurement, the sample was held in a fixture that spun around the axis of illumination at a rate of 14 revolutions per second. Under these circumstances, any birefringence in the sample showed up as a 28-Hz variation in the light intensity sensed by the photodiode. This variation was detected by a lock-in amplifier; the reference phase was provided by an optical chopper that constituted the outer rim of the spinning sample holder. The angular orientation of the chopper with respect to the sample was known, so that the direction of the birefringent slow axis could be determined, as well as the magnitude of the birefringent retardation.

The quarter-wave plate in the above apparatus served to increase greatly the amplitude of the intensity variation sensed by the photodiode. With no quarter-wave plate present, the fluctuation of the transmitted light is very small when the sample rotates, displaying a dependence on the retardation of the sample which is quadratic, and varying at four times the rate of sample rotation. With the quarter-wave plate in place, a linear dependence on retardation is seen, yielding a much larger response, at a frequency twice that of sample rotation. It can be shown that retardation θ (in cycles) of the rotating sample can be determined from the rms variation of the photodiode signal, $V_{\rm rms}$, by

$$\theta = (\sqrt{2}/\pi)\ (V_{\rm rms}/V_0),$$

where V_0 is the photodiode voltage corresponding to maximum transmitted intensity. The use of the quarter-wave plate permits the direction of the slow birefringent axis to be determined unambiguously by comparison of the phases of the photodiode signal and the chopper reference signal.

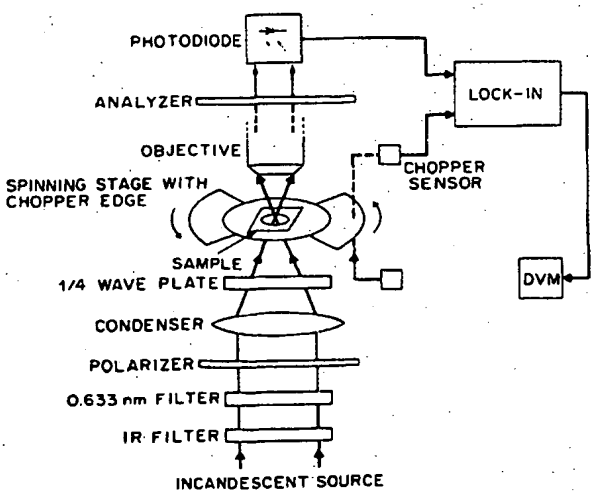

FIG. 2. Apparatus for measurement of birefringence changes of thin polymer films on glass substrates.

B. Measurement procedure

Samples examined with the above apparatus consisted of 2.5×2.5 cm glass plates 1 mm thick (cut from microscope slides) which were coated with a test polymer on one surface. The sample was held in place by a spring clip that exerted a force on the edge of the glass of only 1–2 g. Significantly greater forces were found to induce measurable birefringence in the glass. The sample was square to avoid a similar birefringence due to centrifugal force.

Polymer films were deposited on the glass samples by spinning on dilute (typically 0.5% by weight) polymer solutions and then baking out the solvent. The polymers, their solvents, and the approximate thickness of the resulting films are listed in Table I. Both crystalline and amorphous polymers were chosen so that the effects of crystallinity could be examined. Buffing was performed by pressing the sample down onto a cotton cloth with a weight and moving it unidirectionally over the cloth a fixed distance at a known velocity. The values of pressure and velocity were 7 g/cm^2 and 4 cm/s, respectively. The effects of changing buffing speed were examined, though not extensively. We found no dramatic change in results for buffing speeds from 10 to 0.1 cm/s. A device was employed to move the sample over the cloth so as to produce a repeatable and accurately undirectional motion over a known distance. The uncoated glass samples exhibited a birefringent retardation of their own. Only glass samples showing initial retardation of 4×10^{-4} cycles or lower were used. Coating the glass with the polymers did not alter this initial value.

The measurement procedure was as follows. An initial measurement of retardation of the polymer-coated sample was made. The sample was then buffed by moving it a given distance over the cloth and the retardation was remeasured. The sample was buffed a second time for a second known distance and the retardation was measured once again. This process was continued, yielding a series of retardation values. The buffing-induced retardation as a function of cumulative buffing distance was then computed as the difference between the initial retardation and the retardation observed after each new increment of buffing. For most of the polymers, the buffing-induced retardation was comparable in magnitude to the retardation of the uncoated glass sample itself, so that no substantial decrease in accuracy resulted from the subtraction of the two readings. The integration time constant of the lock-in was 10 s and integration was allowed to continue for 30 s before a reading was made.

TABLE I. List of spun-on polymer films studied in this article.

Polymer	Solvent	Thickness (Å)
Polyethylene-terephthalate (PET)	Chlorophenol	200–300
Nylon 6/6	Chlorophenol	300–400
Polyvinyl alcohol (PVA)	Water	300
Polyformaldehyde (PF)	Chlorophenol	250
Polystyrene (PS)	Methylethylketone	250
Polycarbonate (PC)	Dichloroethane	250
Polymethylmethacrylate (PMMA)	Methylethylketone	350

Readings made in this way for a given sample were repeatable over a period of several minutes to an accuracy of 1×10^{-5} cycles of retardation.

C. Results

A graph summarizing the observed buffing-induced birefringence for the polymer films studied is seen in Fig. 3. Each curve gives the retardation in cycles averaged over three samples, plotted as a function of the cumulative distance of buffing that each sample had experienced. Both positive and negative values of retardation are plotted, with positive values indicating that the slow axis was parallel to the direction of rubbing and negative ones indicating a slow axis perpendicular to the rub axis. The responses generally show a rapid rise in magnitude of retardation followed by a leveling off. Prominent features seen in the figure are the negative retardation values for polystyrene and the lack of any measurable birefringent response for polymethylmethacrylate. In the remainder of this section, we will examine these and other features of the data of Fig. 3 and shown how they further support the hypothesis of buffing-induced polymer chain orientation.

The negative value of retardation for polystyrene, in contrast with the positive values for all of the other polymers, is perhaps the most striking feature seen in Fig. 3. Drawn bulk sheets of all the polymers were tested for magnitude and sense of birefringence. All could be drawn to some extent; polymethylmethacrylate and polystyrene required warming to allow drawing. All but one of the drawn samples exhibited positive retardation, with the slow axis corresponding to the direction of elongation. The exception was polystyrene, which exhibited a negative retardation. This anomalous bulk behavior of polystyrene is reflected clearly in the negative retardation data for this polymer in Fig. 3. It is not clear why this material could only be drawn in bulk when warmed, while room-temperature rubbing of a thin film evidently resulted in deformation. Perhaps the substrate exerted a stabilizing effect, preventing fracture, or perhaps some frictional heating of the film occurred during buffing. Nonetheless, the correspondence of negative retardation in both bulk and rubbed film for this material is striking confirmation of the hypothesis of buffing-induced polymer film orientation.

In the case of polymethlymethacrylate, only negligible birefringence could be induced by drawing at elevated temperatures. This very brittle material either deformed as a highly viscous material (when heated) or it fractured. This bulk drawing behavior corresponds well to the data for polymethylmethacrylate in Fig. 3, where no retardation could be observed. Any notion that the retardation measurement technique was actually measuring a spurious effect caused by scratching of the polymer surface during buffing is refuted by the data for this polymer, since polymethylmethacrylate should be as subject to scratches as the rest of the materials.

It will have been noticed that there is no curve in Fig. 3 for polyfomaldehyde. The buffing-induced birefringence observed in this material decayed rapidly at room temperature and could actually be seen decaying over the 30-s integration time if the measurement was performed promptly after buffing. It was found that the residual birefringence remaining at room temperature decayed to zero when the sample was heated to 40 °C.

All of the polymers that exhibit a birefringent response to buffing also show a tendency to saturate in their response as the buffing process proceeds. Though no rigidly fixed limit is seen in the curves of Fig. 3, the rate of rise does slow dramatically. This effect is understandable if one considers that the tiny areas of contact between the fibrous buffing material and the polymer film constitute only a minute fraction of the surface's area. As buffing proceeds, these isolated contact areas will leave behind narrow "streaks" of deformation in the polymer film (Fig. 4). At first, the contact areas will encounter only virgin surface, and the fraction of the total area that has been affected by buffing will increase linearly. But as the process continues, the streaks will begin to

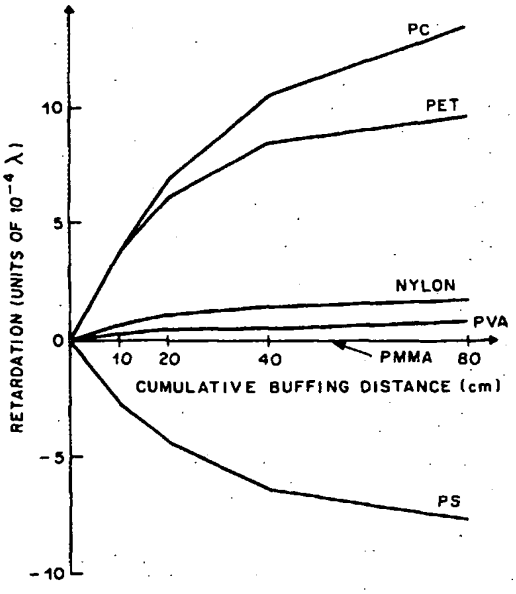

FIG. 3. Plot of retardation induced by buffing. Buffing was performed by pressing the coated sample face down on cotton cloth and pushing it along for a known distance.

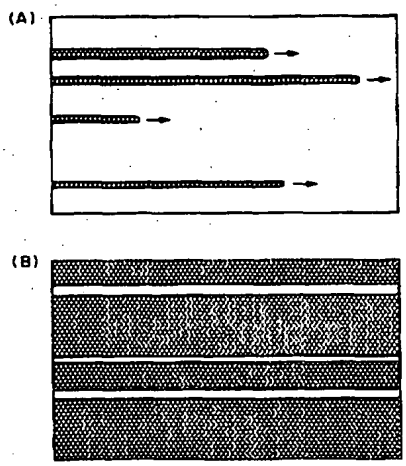

FIG. 4. Accumulation of oriented area of polymer film in streaks as minute regions of contact with the buffing material move across the polymer surface: (a) at beginning of buffing and (b) approaching saturation.

overlap, causing a reduction in the rate at which the buffed area increases. Assuming that most of the deformation that the shearing force at a contact area can cause will occur on first contact, it is then clear that the observed retardation will increase first rapidly, then slow down as more and more of the surface is touched. The plausibility of this streak picture of buffing will be reinforced later in this article.

In Fig. 5, the birefringence, Δn, of the buffed films is plotted against the Δn of the above-mentioned bulk polymer sheets. The maximum retardations recorded in Fig. 3 together with the thickness data of Table I were used to determine Δn for the buffed films. Retardation for the bulk sheets was estimated by fringe counting, observed in 633-nm light, and their thickness was measured with a micrometer after drawing. It can be seen that the Δn for the buffed films is substantially smaller than the Δn for the drawn sheets. It is not clear why the buffed films exhibit smaller birefringence. The reason may relate to the fact that the polymer films are so thin (200–300 Å) that their thickness is substantially less than the length of the polymer molecules themselves. Interactions between the polymer chains and the substrate surface may contribute to an inhibition of chain orientation. For instance, a given chain may come into contact with the substrate surface at a number of points. Any binding to the surface at those points could prevent the full elongation of that chain during buffing. This could give rise to shearing in the polymer layer that was greater near the layer's free surface and smaller near the substrate, as suggested in Fig. 1(d). In spite of the relatively small size of the buffing-induced Δn values, a general trend is evident in Fig. 5, with the materials with large bulk values showing greater film birefringence and those with small bulk values tending to have lesser film birefringence.

D. Further experiments

The above observations indicate that the buffing of thin polymer films induces orientation of the polymer chains in a manner similar to cold drawing of bulk polymer samples. Such orientation offers a straightforward explanation of the birefringence observed. In this section, we describe additional experiments which support the picture of shearing deformation that was proposed in Sec. II as the mechanism by which buffing could induce such polymer chain orientation.

A key feature of the shearing-deformation theory is the idea of a tilting of the polymer material. This motion transforms a rectangular piece of the film (as seen in cross section) into something like a highly elongated parallelogram, as in Fig. 1. On the basis of this picture, it is natural to conclude that if a polymer film so deformed were buffed in the opposite direction, the process of deformation could be reversed and the magnitude of observed retardation would actually decrease. Such an effect has been observed in polyethyleneterephthalate films. Figure 6 shows birefringence data similar to that of Fig. 3 for a polyethyleneterephthalate film. After 80 cm of buffing in one direction, several additional increments of buffing were performed in the opposite direction. It can be seen that the magnitude of measured retardation decreases significantly, followed by a leveling off. However, if only 10 or 20 cm of buffing in the initial direction were performed, no such decrease was seen.

The above effects of reversed buffing are understandable in light of the "streak" picture of buffing. If only a small amount of initial-direction buffing is performed, then only a minority of the surface's area will consist of streaks of oriented material. Reversed direction buffing will produce new streaks of orientation primarily in untouched areas. No compensation will occur between these two oriented areas, since both represent polymer elongation along essentially the same axis. However, if a surface is thoroughly buffed initially, almost all of its surface will be oriented. During reversed buffing, the tiny areas of contact between the surface and the buffing material will now be likely to overlap with previously oriented material. With overlap occurring, the reversed buffing can act either to reduce the tilted deformation of film or to reverse its direction. In Fig. 6, reduction of tilt seems to occur at first, with consequent lowering of retardation magnitude. Evidently, as reversed buffing continues, actual reversal of the direction of sheared deformation begins to occur so that as old areas of tilt are lost, new ones of equal and opposite tilt are generated. These both contribute equally to retardation, explaining the leveling off seen in the curves of Fig. 3. All of this seems to confirm both the concept of shear

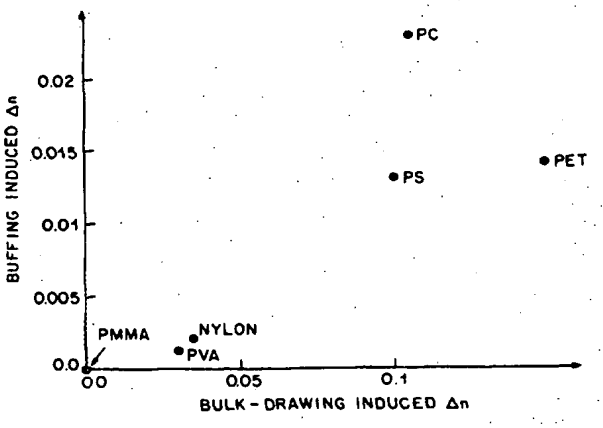

FIG. 5. Plot of magnitude of Δn measured from buffed polymer films vs magnitude of Δn measured from drawn bulk samples of the same polymers. The abbreviations for the polymers are the same as those given in Table I.

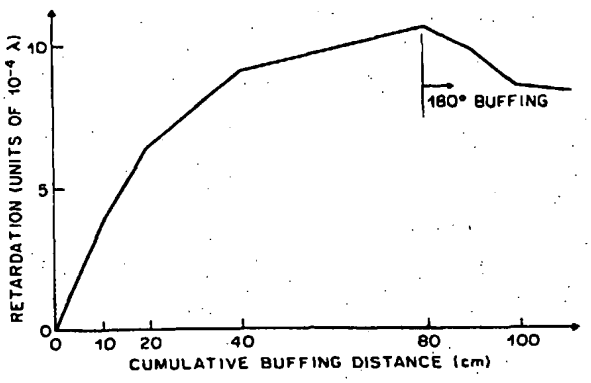

FIG. 6. Plot of retardation of a PET film buffed first in one direction and then in the opposite direction.

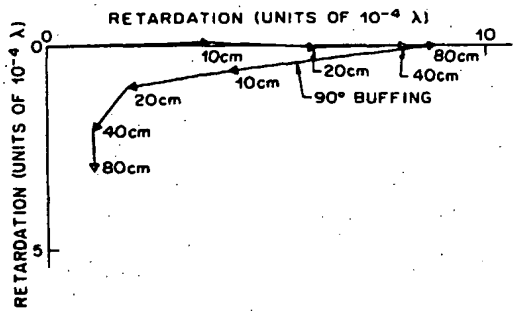

FIG. 7. Polar plot showing magnitude and direction of the slow axis of birefringence of a PET film buffed first in one direction and then at 90° to that direction. Both axes are labeled with the radial scale factor for retardation magnitude. There is no sense associated with the slow axis; the sense of the plotted points was chosen arbitrarily for convenience of display.

deformation induced by buffing and the idea that this deformation occurs by the accumulation of individual streaks caused by the motion of minute areas of contact between surface and the buffing material.

A second experiment, also involving rebuffing of the polymer surface, was performed. A surface coated with polyethyleneterephthalate was initially buffed in a given direction and then buffed at 90° to that direction. The results of this experiment are seen in the plot of Fig. 7. The plot shows in polar form the magnitude of the measured retardation and the angular orientation of its slow axis. (There is no sense associated with this axis and the sense of the plotted points in Fig. 7 was chosen arbitrarily. The sequence in which the data points were taken is indicated by arrows.) It can be seen that the birefringence that accumulated in the initial buffing decreases nearly to zero, followed by a renewed accumulation along the new buffing axis. Some skewing of the birefringent axis toward the direction of initial buffing remains, about 19°.

These results are also understandable in terms of the picture of polymer deformation developed in Sec. II. A bulk polymer sample can be redrawn in a direction normal to that in which it was initially cold drawn, with resulting polymer chain orientation along the new drawing axis. In light of the model, rebuffing of a thin polymer film can be expected to turn the axis of orientation by 90° along streaks of contact between the polymer and the fibrous buffing material. Being at right angles, the new and old regions of orientation tend to compensate each other in the spatially averaged birefringence measurements. Thus, as streaks of new orientation accumulate, the net retardation will diminish until the new orientation areas constitute 50% of the surface. Magnitude of retardation will then be close to zero. Further accumulation of new streaks causes the retardation magnitude to again increase, with opposite sign. With continued buffing, the streaks of new polymer orientation begin to overlap until the whole surface of the polymer is reoriented. This sequence parallels the trajectory of the "retardation vector" in Fig. 7. The small displacement of the final points toward the right-hand side of the vertical axis can be explained as a lingering contribution from the initial orientation that is not fully reoriented by rebuffing. This contribution could be due to the deeper portions of the polymer layer, perhaps work hardened by the initial deformation, which fail to reorient. The net observed birefringence would be the combination of a persistent contribution in the original direction plus the contribution of the reoriented upper portion of the layer. Alignment results described in Sec. IV B suggest that the upper portion may be fully reoriented in the new direction.

IV. RELATION BETWEEN POLYMER ORIENTATION AND LIQUID-CRYSTAL ALIGNMENT

In the previous section, we have established that buffing of a thin polymer film can cause the orientation of the molecular chains of the polymer. We have also shown that such orientation occurs through a shearing deformation of the film and that this deformation accumulates in narrow streaks as buffing proceeds. We now wish to examine how some buffed polymers surfaces can interact with liquid-crystal materials to produce alignment. In the subsections below, we will discuss the aligning abilities of specific polymers, show that when alignment occurs it is caused by the oriented polymer and not by other effects such as surface scratches, and offer evidence that polymer crystallinity is necessary for alignment to occur. Finally, we will propose the view that the aligning influence of the buffed polymer acts on the liquid crystal in a way analogous to epitaxy in solid crystal materials.

A. Alignment capabilities of the test polymers

Polymer films identical to those studied in Sec. III were spun onto pairs of indium tin oxide-coated glass plates. The polymer surfaces were buffed at a pressure of 15 g/cm^2 for a total distance of 40 cm on cotton cloth identical to that used previously. The pairs of plates were assembled with buffing axes parallel to form cells. The spacing was set at 5 μm by the use of glass fiber spacers. Cells were made for each of the polymers studied in Sec. IV and each were tested for its ability to align both a smectic and a nematic mixture. The smectic mixture was composed of two chiral esters synthesized[10,11] by Goodby:

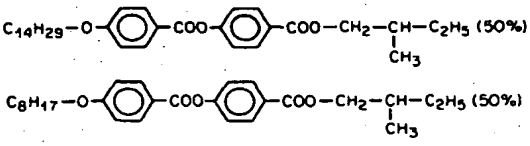

This material exhibits the isotropic–to–smectic-A phase sequence with transition temperature of 56 °C. It was selected because of its room-temperature smectic-A range and because the isotropic–to–smectic-A transition is especially favorable for producing alignment. The nematic was the commercial mixture E80, manufactured by BDH, with an isotropic-to-nematic transition at 60 °. The cells were filled in the isotropic state and cooled. Texture formation was observed by polarized light microscopy as cooling proceeded. Experience with other materials has shown that alignment results do not vary dramatically from one nematic or smectic to another and the results with these two materials were taken as typical of each class of material.

The results of the alignment tests are summarized in Table II. The polymers fall into two broad categories. Those

TABLE II. Alignment obtained with various buffed polymer films.

Polymer	Smectics		Nematics	
	Aligns	No alignment	Aligns without defects, sheet nucleation	Aligns with defects, point nucleation
Polyethylene-terephthalate	×		×	
Nylon 6/6	×		×	
Polyvinyl alcohol	×		×	
Polyformaldehyde		×		×
Polystyrene		×		×
Polycarbonate		×		×
Polymethylmethacrylate		×		×
Bare glass		×		×

listed first in the table seem to exert a strong aligning influence. They are the only ones of the polymers that align the smectic material at all. As the cell is cooled, nucleation of aligned smectic-*A* material is observed to occur in numerous elongated patches which grow until they fill the cell. With polymers of the second category, the smectic-*A* phase nucleates at numerous tiny points and grows out into the cell along a different axis of alignment from each point, with no discernable preference for the buffing direction. With the nematic material, alignment of some quality is observed for all the polymers. However, with polymers of the first category, "sheet nucleation" on the cell surfaces is observed as the nematic phase is entered. These nematic layers grow in thickness until they meet in the center of the cell, producing a flaw-free aligned texture. With polymers of the second category, the nematic phase nucleates in numerous isolated spots whose alignment is either random or is only loosely correlated with the buffing axis. As the spots grow and join, their alignment axes change and become oriented parallel to the buffing axis. Disclinations generally remain, disrupting the alignment. Thus, although an aligned texture is attained, the aligning influence exerted by polymers of the second category on nematics is of a weaker kind than that exerted by polymers of the first category.

Additional cells were fabricated, buffed like the others, but lacking any polymer coating. They were found to align the nematic material like the cells with surface coatings of the second-category polymers. This implies that the second-category polymers exert no aligning influence of their own and that their relatively weak aligning abilities are due to other effects of buffing. These cells were incapable of producing any alignment of the smectic material and thus again resembled the cells with second-category coatings. These results, together with those of the previous paragraph, indicate that only polymers of the first category are capable of exerting an aligning influence of their own, over and above the influence of buffing itself in the absence of any polymer coating. Hence, only polymers of the first category seem capable of "polymer alignment," with second-category polymers showing no behavior substantially different from an uncoated cell surface.

Examining the properties of the two categories of polymers, the distinction between the two categories becomes evident: those of the first category are highly crystalline materials, while those of the second category are strongly amorphous. The only exception is polyformaldehyde, which is highly crystalline, yet caused no alignment of the smectic material and caused only the weaker form of alignment in the nematic material. As reported in Sec. III, this polymer exhibited complete relaxation of buffing-inducing birefringence at 40 °C and some relaxation could even be seen at room temperature as the retardation measurements were being made. Since the cells were filled at temperatures above the clearing points (56 and 60 °C) of the test materials, the polyformaldehyde coating should have been fully relaxed and thus should have not caused alignment. Thus, the differences in alignment ability of the two categories of polymer seem to correlate (in all cases where polymer orientation was retained during filling) with the crystallinity of the polymer. Consequently, both polymer chain orientation and polymer crystallinity appear to be necessary conditions for alignment, and neither is sufficient alone.

B. Alignment by bulk cold-drawn polymers

Before examining further the significance of polymer crystallinity, we would like to establish the causal link between polymer chain orientation and liquid-crystal alignment. Specifically, we want to show that the strong alignment exhibited by first-category polymers (1) can be produced by polymer chain orientation and (2) cannot be produced by other effects of the buffing process.

To establish the first point above, cells consisting of small samples of bulk cold-drawn polymer films pressed gently against a bare glass surface were fabricated. The glass surface was sprayed with 5-μm glass fibers. Since the polymer films were somewhat warped after drawing, spacing varied greatly, but with a 5-μm minimum. The cells were filled in the isotropic phase with both the nematic and smectic mixtures. Table III shows the polymers used and the alignment obtained. Alignment, when it occurred, was somewhat poorer in quality than obtained by buffing the thin polymer films, but could be clearly seen. Alignment is reported for the minimum thickness portions of the cells, where the best alignment was generally observed. With the smectic material, it can be seen that the results mimic sub-

TABLE III. Alignment obtained in cells made from cold-drawn polymer sheets.

Polymer	Smectics		Nematics	
	Aligns	No alignment	Aligns	No alignment
Polyethylene-terephthalate	×		×	
Nylon 6/6	×		×	
Polystyrene		×		×
Polycarbonate		×		×

stantially the alignment obtained with the same polymers in the conventional cells. The crystalline polymers align the smectic, but the amorphous polymers do not. Since the surfaces of these polymer samples were not buffed or rubbed in any way, it is clear that the observed liquid-crystal alignment must have been a consequence of polymer orientation alone. With the nematic material, alignment can again only be obtained with the crystalline polymers.

The above results show that chain alignment of crystalline polymers is clearly capable of causing alignment in the complete absence of any buffing. We now need to demonstrate that other consequences of buffing are not capable of producing the alignment results that the crystalline polymers are able to produce. The prime candidate for such an effect is the formation of very fine mechanical scratches or grooves on the polymer surface by the buffing process. However, all of the polymers tested should be liable to such surface damage. Yet none of the amorphous materials could exert an aligning effect any stronger than that resulting from the buffing or a bare cell surface. Thus, it appears that, even if scratching or grooving occur, they are incapable by themselves of producing the observed alignment. This was confirmed by an experiment in which a cell was assembled using surfaces that had been buffed and then rebuffed at a 90° angle to the initial buffing direction, like the sample presented in Fig. 7. The polymer used was polyethyleneterephthalate, the buffing distance was 40 cm for both buffs, and the cell spacing was 5 μm. With both smectic and nematic alignment, it was found that the effect of the initial buff was fully overwhelmed by the second one, so that the liquid-crystal molecules were now parallel with the direction of the second buff. If the alignment were caused by scratching, one would expect a fine network of criss-crossing scratches to be produced which would be ineffective at producing a good aligned texture.

C. Polymer alignment as a form of epitaxy

The evidence presented in the above section makes it clear that chain orientation in crystalline polymers is responsible for the strong alignment that those polymers produce. We now want to address briefly the question of how such polymers interact with liquid-crystal materials to cause alignment. Liquid crystals, as their name implies, share some of the properties of conventional solid crystals. In polymer alignment, when the liquid-crystal phase begins to form from the isotropic, it nucleates on the polymer surfaces (either as a sheet as with nematics or in elongated patches as with smectics) and grows out into the bulk of the cell. Thus, the formation of one "crystalline" material, the liquid-crystal phase, has been initiated on the surface of another crystalline material, the oriented polymer, and at least one crystal property, the direction of the molecular axes, has been preserved from one material into another. To this extent, the alignment process resembles epitaxy of conventional solid crystals. Of course, in solids very exact conditions of lattice match generally must be met for epitaxy to occur. But with liquid crystals it is plausible that their much less rigid crystal order would make them much more accommodating of mismatch between substrate and "epi." The liquid-crystal molecules would see the crystalline substrate as resembling an already formed liquid-crystal phase and act as though extending that phase further in space.

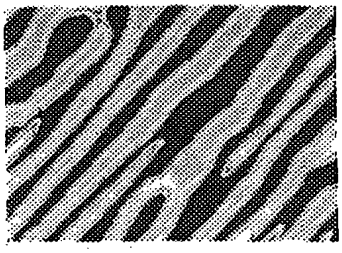

FIG. 8. Micrograph of partially formed smectic texture.

Observation of the transition from isotropic to aligned smectic A tends to support the above picture. Figure 8 shows a 9-μm-thick glass cell with rubbed PET on one face and polystyrene on the other. The cell was filled with the second of the two ester materials described above. The micrograph was taken between crossed polarizers. The black areas are portions of the cell where all of the material is isotropic. The light areas are aligned smectic A (with the rub axis at 45° to the polarizer axis), showing the streaked appearance that is typically observed during A-phase formation with polymer alignment. The birefringence of the aligned material gives rise to light and dark bands around the borders of the streaks that map out the thickness of the smectic material. Visual examination of the sample's behavior as the smectic texture forms indicate that the material is thin at the edges of the streaks and becomes thicker in the center, where it eventually touches the opposite face of the cell. The uniform gray areas in the interior portions of the streaks are the areas of contact.

Figure 9 shows qualitatively a cross-section view of the cell deduced from micrographs like that of Fig. 8. It can be

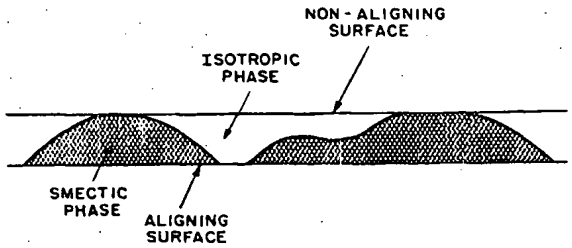

FIG. 9. Typical qualitative cross-section view of cell during formation of smectic texture, as deduced from observation of birefringent contours.

seen that the smectic material preferentially wets the aligning surface relative to the isotopic material. The polystyrene-coated surface shows just the opposite behavior and is wetted preferentially by the isotropic material relative to the smectic material. Since it is generally true that substances that wet each other tend to be similar, these wetting affinities suggest that the isotropic material bears a resemblance to the polystyrene surface, and that the smectic material bears a resemblance to the aligning surface. This makes sense in light of the epitaxy analogy which suggests that the smectic and aligning surface are alike in their being crystalline. The wetting affinity of the isotropic material and the polystyrene surface also make sense since these materials are alike in their being amorphous and noncrystalline.

[1] J. S. Patel, T. J. Leslie, and J. W. Goodby, Ferroelectrics **59** 137 (1984).
[2] J. Cognard, "Alignment of Nematic Liquid Crystals and Their Mixtures," Mol. Cryst. Liq. Cryst. **51**, 1 (1982).
[3] D. W. Berreman, Phys. Rev. Lett. **28**, 1683 (1972).
[4] D. W. Berreman, Mol. Cryst. Liq. Cryst. **23**, 215 (1973).
[5] J. A. Castellano, Mol. Cryst. Liq. Cryst. **94**, 33 (1983).
[6] K. Kondo, H. Takezoe, A. Fukuda, and E. Kuze, Jpn. J. Appl. Phys. **22**, L85 (1983).
[7] H. Aoyama, Y. Yamazaki, N. Matsuura, H. Mada, and S. Kobayashi, Mol. Cryst. Liq. Cryst. **72**, 127 (1981).
[8] M. E. Becker, R. A. Kilian, B. B. Kasmowski, and D. A. Mlysnski, Mol. Cryst. Liq. Cryst. **132**, 167 (1986).
[9] N. A. Clark, Phys. Rev. Lett. **55**, 292 (1985).
[10] J. W. Goodby and T. M. Leslie, *Liquid Crystals and Ordered Fluids*, edited by A. C. Griffin and J. F. Johnson (Plenum, New York, 1984), Vol. 4, p. 1.
[11] J. W. Goodby and T. M. Leslie, Mol. Cryst. Liq. Cryst. **110**, 175 (1980).

Jpn. J. Appl. Phys. Vol. 34 (1995) pp. L 503–L 506
Part 2, No. 4B, 15 April 1995

Effect of the Polymer Tilt Angle for Generation of Pretilt Angle in Nematic Liquid Crystal on Rubbed Polyimide Surfaces

Dae-Shik SEO*, Kazuo ARAYA, Norihiro YOSHIDA, Michinori NISHIKAWA[1], Yoshikazu YABE[2] and Shunsuke KOBAYASHI

Division of Electronic and Information Engineering, Faculty of Technology, Tokyo University of Agriculture and Technology, 2-24-16 Nakamachi, Koganei, Tokyo 184, Japan
[1]*Tokyo Research Laboratory, Japan Synthetic Rubber Co., Ltd., 3-5-1 Higashi-Yurigaoka, Asao-Ku, Kawasaki, Kanagawa 215, Japan*
[2]*Development Engineering Department, Fujitsu Kiden Co., Ltd., 1776 Yanoguchi, Inagi, Tokyo 206, Japan*

(Received October 5, 1994; revised manuscript received January 31, 1995; accepted for publication March 18, 1995)

We have studied the effect of the polymer tilt angle for pretilt angle generation in nematic liquid crystal, 4-cyano-4′-n-penthylbiphenyl (5CB) on rubbed polyimide surfaces. The polymer tilt angle was determined by measuring induced optical retardation produced in rubbed polyimide (PI) surfaces by rubbing. We suggest that the polymer tilt angle is not related directly to the pretilt angle on rubbed PI surfaces by rubbing. We proposed a microscopic model of pretilt angle generation on rubbed PI surfaces by rubbing. Finally, we conclude that the pretilt angle generation of 5CB strongly depends on the characterization of polymer materials and the micro-asymmetric triangular structure of the polymer on rubbed polyimide surfaces.

KEYWORDS: polymer tilt angle, pretilt angle, nematic liquid crystal, polyimide, optical retardation

1. Introduction

Uniform alignment of liquid crystals (LCs) on treated substrate surfaces is very important for both LC fundamental research and applications.[1)] Among the LCs surface alignment techniques, the rubbing method has been most widely used, however detailed mechanism of LC alignment on rubbed PI surfaces is not yet fully understood. In the surface alignment of LCs to prepare an LC cell, it is necessary to generate pretilt angle in a cell in order to avoid the creation of disclinations. The pretilt angle is also important matter in order to avoid the stripe domain on super twisted nematic liquid crystal displays (STN-LCD)[2)] and surface-stabilized ferroelectric liquid crystal display (SSFLCD).[3)] The generation of pretilt angle in nematic liquid crystals (NLCs) on alignment layers by unidirectional rubbing was demostrated and discussed by many investigators.[4–12)]

Recently, we reported the aligning capabilities of the NLC, 5CB, on rubbed PI,[7–12)] polypyrrole (PP),[13)] PI Langmuir-Blodgett (LB),[14)] polystyrene (PS),[15)] and PI containing trifluoromethyl moieties.[10)] Geary *et al.* reported the orientation of polymers for LC alignment on various alignment layers by the rubbing process.[5)] Recently, Han *et al.* reported the relationship between the polymer tilt angle and the pretilt angle in NLC on rubbed PI surfaces by rubbing.[16)]

In this paper, we report the effects of the polymer tilt angle for generation of pretilt angle in 5CB on various rubbed PI surfaces by rubbing.

2. Experimental

The PI materials, studied were:

RN-626 (PI, Nissan Chemical Industries Co., Ltd.)
: Containing trifluoromethyl moiety and low polarization.

SE-150 (PI, Nissan Chemical Industries Co., Ltd.)
: With side chain and medium polarization.

RN-305 (PI, Nissan Chemical Industries Co., Ltd.)
: Without side chain and highest polarization.

The precursors were coated on indium-tin-oxide (ITO)-coated glass substrates, and imidized at 250°C for one hour. The PI films were rubbed using a machine equipped with a nylon roller (Y_o-15-N, Yoshikawa Chemical Industries Co., Ltd.). The definition of the rubbing strength, RS, was given in previous papers[8–10)] The LC was assembled in cells with antiparallel-rubbed surfaces. The polymer tilt angle was defind by measuring the optical retardation measurement system as shown in Fig. 1. The light source is a He–Ne laser (632.8 nm) with 2 mW output, an acoustic modulator, and an analyzer and the output signal is detected by a photodiode. We defined that the polymer tilt angle is symmetric point of optical retardation for 0 deg of angle of incidence on rubbed surfaces. The pretilt angle of the LC media in the nematic phase were measured using the crystal roation method.[17)]

3. Result and Discussion

Figure 2(a) shows the induced optical retardation (afler rubbing value-bare ITO value) of the rubbed PI surface (SE-150) as a function of angle of incidence by rubbing. The polymer tilt angle is 0 for $RS=0$, but the polymer tilt angle increases with the RS. Figure 2(b) shows the induced optical retardation (after rubbing value-bare ITO value) of the rubbed PI surface (RN-305) as a function of angle of incidence by rubbing. The polymer tilt angle is about 0 for all RS. Figure 3 shows the polymer tilt angle on three kinds of the rubbed PI surfaces as a function of RS. It is shown that the polymer tilt angle is 0 for all $RS=0$ on three kinds of PI surfaces. We consider that the polymer tilt angle is parallel for unrubbed PI surfaces. The polymer tilt angle increases with the RS, on PI surfaces (SE-150 and RN-626) but does not increase on PI surface (RN-305)

*Present address: Liquid Crystal Institute, Kent State University, Kent, Ohio 44242, USA.

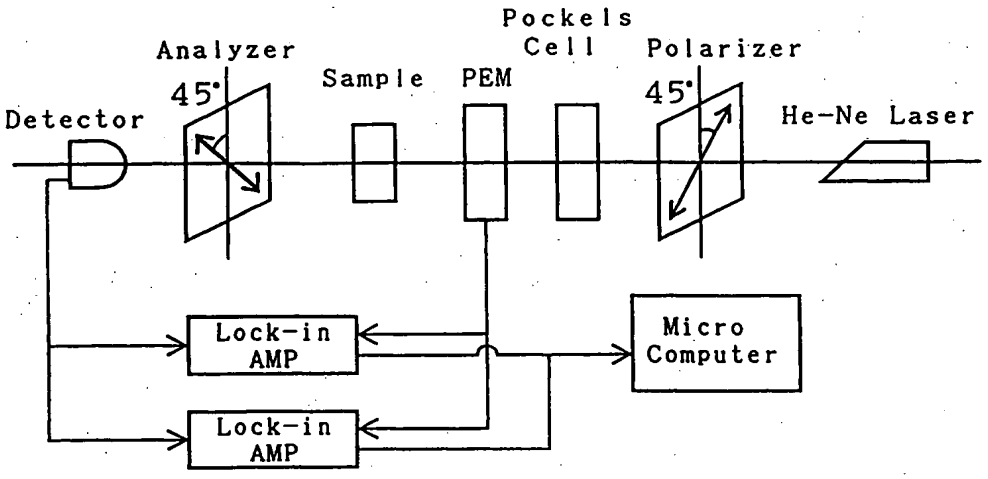

Fig. 1. The measurement system of the optical retardation.

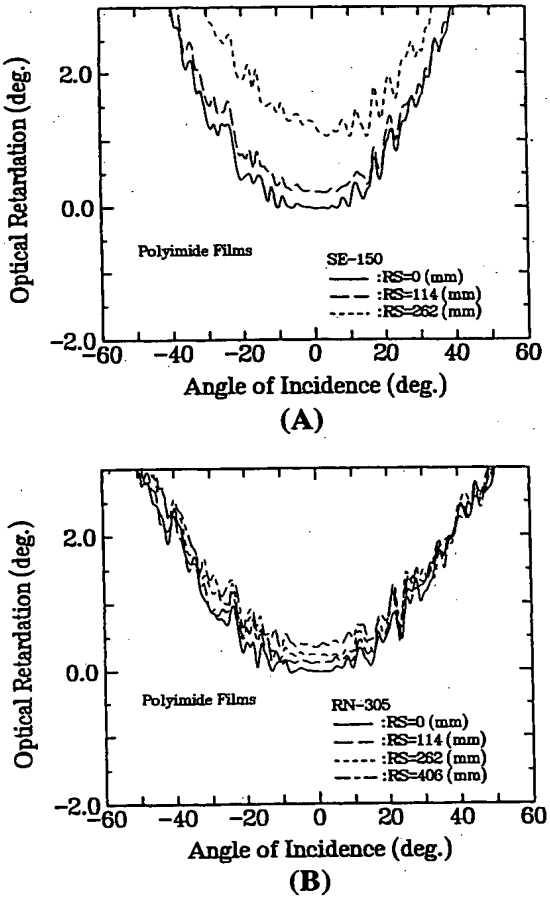

Fig. 2. Induced optical retardation produced in rubbed PI surfaces as a function of angle of incidence. PI are (a) SE-150; (B) RN-305.

with the *RS*. From these results, we suggest that the polymer tilt angle strongly depends on the polymer materials.[18] We consider that the polymer tilt angle on rubbed PI surface indicates the easy axis of the polymer on PI surface by rubbing. Therefore, we conclude that the easy axis of the polymer on rubbed PI surfaces strongly depends on the polymer materials.

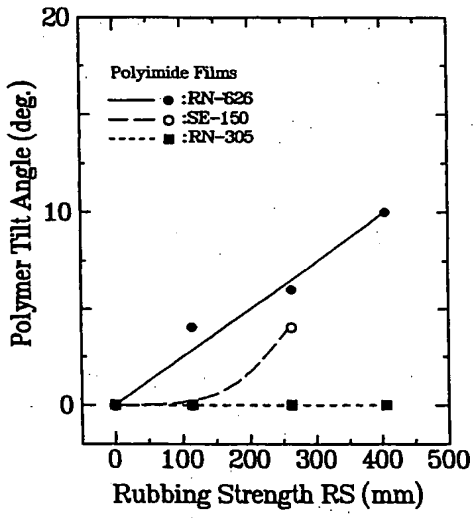

Fig. 3. The polymer tilt angle on three kinds of the rubbed PI surfaces as a function of *RS*.

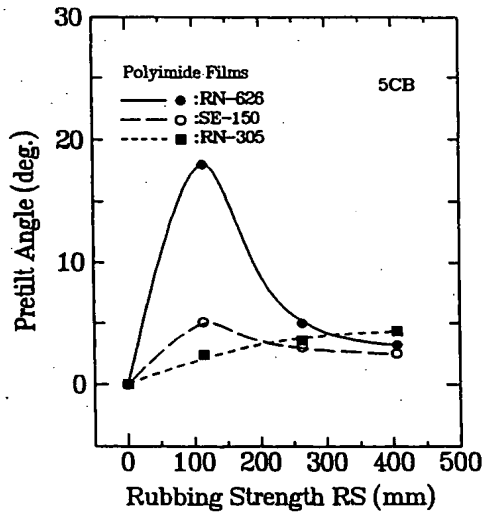

Fig. 4. The pretilt angle in 5CB on three kinds of the rubbed PI surfaces as a function of *RS*.

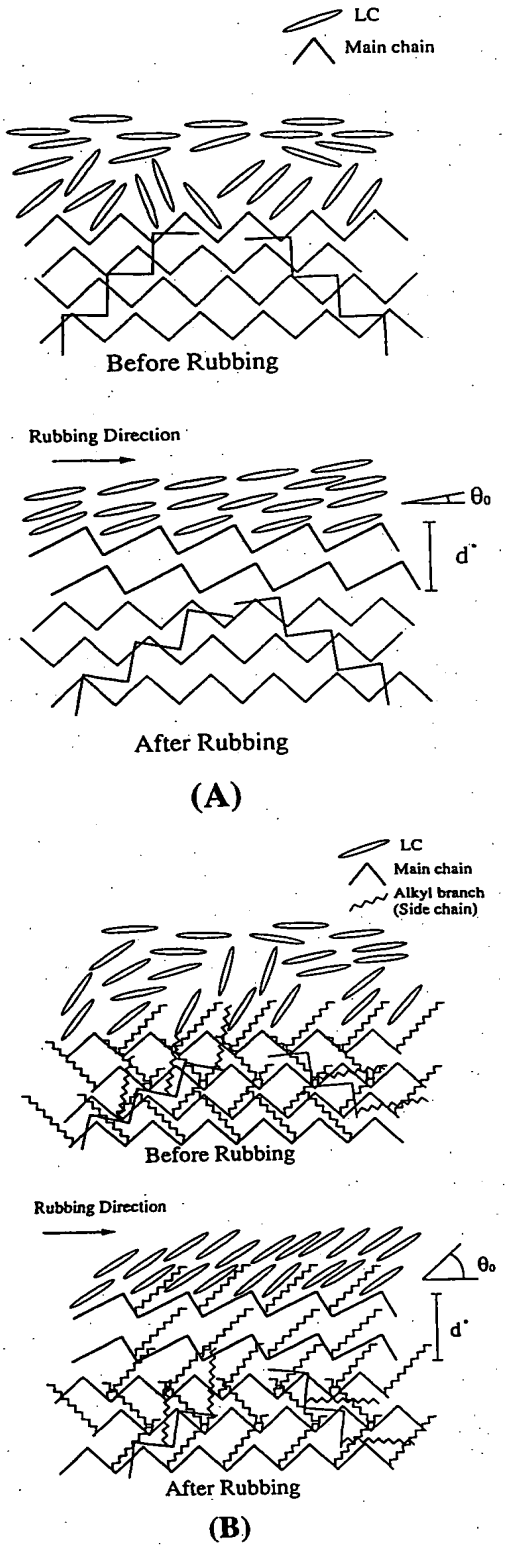

Fig. 5. The microscopic model of the pretilt angle generation on rubbed PI surfaces. (a) Without side chain; (b) With side chain.

Figure 4 shows the pretilt angle of 5CB on three kinds of the PI surfaces as a function of *RS*. The pretilt angle of 5CB on rubbed PI surface (RN-626) is very high for weak *RS*, and decreases with the *RS*. The pretilt angle of 5CB on rubbed PI surface (SE-150) increases with the *RS*, and decreases with the *RS*. In PI surface (RN-305), the pretilt angle of 5CB increases with the *RS*, however, the polymer tilt angle increases with the *RS* for wide range of *RS* on PI surfaces (SE-150 and RN-626). From these results, we suggest that the polymer tilt angle is not related directly to the pretilt angle on three kinds of rubbed PI surfaces.

Figure 5 shows the microscopic model of the pretilt angle generation on rubbed PI films without side chain and with side chain. Before rubbing treatment, we consider that the PI chains show the Zig-Zag conformation, and the PI chain show the circle conformation.[19-20] After rubbing treatment, PI chain generates the expansion of the PI chain and then show asymmetric triangular structure for rubbing direction.[19-20] The pretilt angle is generated by micro-asymmetric triangular structure of the polymer on rubbed PI surface without side chain by rubbing in Fig. 5(a). In Fig. 5(b), the pretilt angle is generated by combination of the micro-asymmetric triangular structure of the polymer and the side chain on PI film having side chain by rubbing. In Fig. 5 (b), we suggest that the pretilt angle in NLC is generated by micro-surface excluded volume effect on rubbed PI film having side chain.[7]

Finally, we conclude that the pretilt angle generation of 5CB strongly depends on the characterization of the polymer materials[9,10] and the micro-asymmetric triangular structure of the polymer on alignment layers.

4. Conclusions

We investigated the effect of the polymer tilt angle for pretilt angle generation of the NLC aligned on three kinds of PI surfaces. That the polymer tilt angle is not related directly to pretilt angle on rubbed PI surfaces by rubbing is suggested. We proposed the microscopic model of pretilt angle generation on rubbed PI surfaces by rubbing. Finally, we conclude that the generation of pretilt angle in 5CB strongly depends on the characterization of the polymer materials and the micro-asymmetric triangular of structure of the polymer on rubbed polyimide surfaces.

Acknowledgment

The authors wish to acknowledge H. Fukuro of Nissan Chemical Industries Co., Ltd. for providing PI materials and Dr. J. West of Liquid Crystal Institute of Kent State University for the reading of the manuscript and for suggestions. This work was partially supported by the Foundation of Ando Laboratory and by a Grant-in-Aid for Encouragement of JSPS Junior Scientists from the Ministry of Education, Science and Culture.

1) J. Cognard: Mol. Cryst. & Liq. Cryst. **78**, Suppl. 1 (1982) 1.
2) T. J. Scheffer and J. Nehring: Appl. Phys. Lett. **45** (1984) 1021.
3) N. A. Clark and S. T. Largerwall: Appl. Phys. Lett. **36** (1980) 899.
4) M. E. Becker, R. A. Kilian, B. B. Kosmowski and D. A. Milynsky: Mol. Cryst. & Liq. Cryst. **130** (1986) 167.
5) J. M. Geary, J. W. Goodby, A. R. Kmetz and J. S. Patel: J. Appl. Phys. **62** (1987) 4100.

6) S. Kuniyasu, H. Fukuro, S. Maeda, K. Nakaya, M. Nitta, N. Ozaki and S. Kobayashi: Jpn. J. Appl. Phys. **27** (1988) 827.
7) T. Sugiyama, S. Kuniyasu, D.-S. Seo, H. Fukuro and S. Kobayashi: Jpn. J. Appl. Phys. **29** (1990) 2045.
8) D.-S. Seo, K. Muroi and S. Kobayashi: Mol. Cryst. & Liq. Cryst. **213** (1992) 223.
9) D.-S. Seo, H. Matsuda, T. Oh-ide and S. Kobayashi: Mol. Cryst. & Liq. Cryst. **224** (1993) 13.
10) D.-S. Seo, S. Kobayashi and M. Nishikawa: Appl. Phys. Lett. **61** (1992) 2392.
11) D.-S. Seo, T. Oh-ide, H. Matsuda, T. Isogami, K. Muroi, Y. Yabe and S. Kobayashi: Mol. Cryst. & Liq. Cryst. **231** (1993) 95.
12) D.-S. Seo, Y. Iimura and S. Kobayashi: Appl. Phys. Lett. **61** (1992) 234.
13) D.-S. Seo, S. Kobayashi and A. Mochizuki: Appl. Phys. Lett. **60** (1992) 1025.
14) D.-S. Seo, T. Oh-ide and S. Kobayashi: Mol. Cryst. & Liq. Cryst. **214** (1992) 97.
15) D.-S. Seo, K. Muroi, T. Isogami, H. Matsuda and S. Kobayashi: Jpn. J. Appl. Phys. **31** (1992) 2165.
16) K.-Y. Han, P. Vetter and T. Uchida: Jpn. J. Appl. Phys. **32** (1993) L1242.
17) T. J. Scheffer and J. Nehring: J. Appl. Phys. **48** (1977) 1783.
18) D.-S. Seo, K. Araya, N. Yoshida, S. Kobayashi and M. Nishikawa: *Proc. 19th Japanese Liquid Crystal Conf.* (1993) p. 110.
19) S. Kobayashi and Y. Iimura: Proc. SPIE **2175** (1994) 122.
20) M. Nishikawa, N. Bessho, T. Natsui, Y. Ohta, N. Yoshida, D.-S. Seo, Y. Iimura and S. Kobayashi: submitted to Mol. Cryst. & Liq. Cryst. (1994).

Flexoelectric Electro-optics of a Cholesteric Liquid Crystal

J. S. Patel
AT&T Bell Laboratories, Murray Hill, New Jersey 07974

and

Robert B. Meyer
The Martin Fisher School of Physics, Brandeis University, Waltham, Massachusetts 02254
(Received 18 December 1986)

A linear electro-optic effect in a cholesteric liquid crystal is described and attributed to the flexoelectric effect. An electric field applied perpendicular to the helix axis rotates the director about an axis parallel to the field. This produces a periodic splay-bend pattern in the helix, which couples flexoelectrically to the field.

PACS numbers: 61.30.Gd, 78.20.Jq

The helical structure of a cholesteric liquid crystal can be modified or even completely unwound by an applied electric field. This is well understood in terms of the coupling of the electric field to the dielectric anisotropy of the liquid crystal, an effect which is quadratic in the amplitude of the electric field. In this Letter, a new effect is described which is linear in the electric field, and therefore arises from a different coupling mechanism. Following a description of the observations, an explanation is proposed in terms of the linear flexoelectric effect, which accounts for all the experimental observations, and predicts some other properties that can be tested.

The phenomenon is readily observed in a uniformly aligned parallel-plate cell in which the helical axis of the cholesteric lies parallel to the glass surfaces in a unique direction. The inner surfaces of the cell are coated with transparent electrically conductive layers so that an electric field can be applied perpendicular to the plates and to the helix axis. When such a cell is observed between crossed polarizers, extinction is observed whenever the helix axis is parallel or perpendicular to the polarizer, since macroscopically a small-pitch cholesteric acts like a uniaxial crystal with the helix as its optical axis. In this extinction configuration, when a small electric field is applied, the cell transmits light, indicating a rotation of the optical axis in the plane of the cell. By rotation of the cell through a small angle, extinction is once again achieved. It is found that the rotation direction changes with the polarity of the field and the rotation angle is linear in the field amplitude, at least for small fields.

This effect has been observed in several different cholesterics. Figure 1 displays results for *S*-4-*n*-nonyloxyphenyl-4'-(3",7"-dimethyloctyloxybenzoyloxy) benzoate, in a cell approximately 2.75 μm thick and with indium-tin oxide electrodes coated with poly-1,4-butyleneterephthalate to produce parallel molecular alignment at the surface.[1] Initial alignment of the helix axis parallel to the glass was achieved by cooling of the sample from the isotropic state in the presence of an electric field. Because this material has a positive dielectric anisotropy, this orientation of the helix has the lowest dielectric energy. This geometry should produce a fingerprint texture. However, this texture was not visible at low fields, in the material being examined, because of the short pitch comparable to the wavelength of the light. It was nevertheless clearly evident in the presence of an electric field at values close to the unwinding voltage. Measurements of the effect were then made with a 40-Hz square wave of variable amplitude, monitoring the

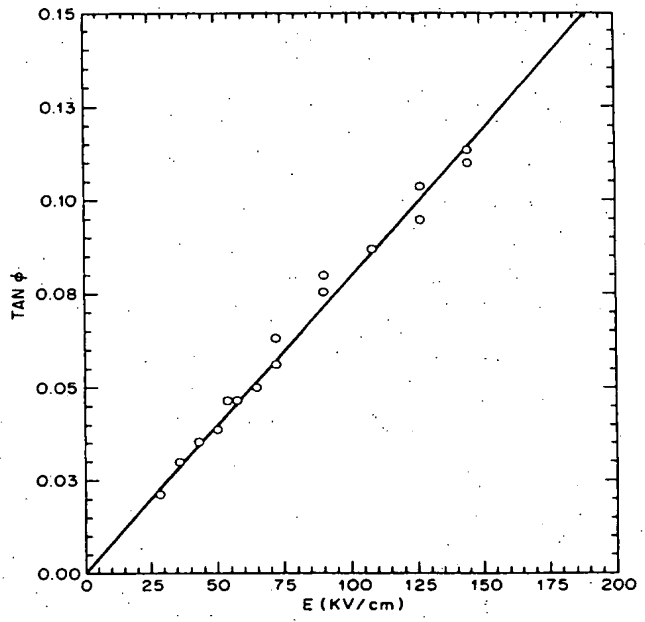

FIG. 1. Rotation of the optical axis (tanϕ) vs applied field (E).

transmitted light intensity with a photodiode and an oscilloscope. For each field amplitude the cell was rotated clockwise and counterclockwise to find the extinction angles for each polarity of field. The dependence of rotation angle on field is linear up to the field at which the dielectric coupling results in unwinding the helix. Although this effect is clearly observed in thicker samples (14 μm), the poor quality of alignment prevented quantitative measurements in these samples for this material.

It is proposed that these observations are explained by the flexoelectric effect, which is a linear coupling between an electric polarization and splay and bend deformations of the liquid crystal. Although the flexoelectric effect has been known and studied for a long time, it has played a secondary role in the phenomenology of liquid crystals because of its complex geometrical requirements. It is most easily observed when either the liquid crystal[2,3] or the electric field[4] is highly inhomogeneous in orientation. The present case is no exception in this regard, although it is simpler in practical respects than other flexoelectric phenomena.

One of the first flexoelectric phenomena proposed by Meyer[5] is one in which a uniform electric field induces the formation of a continuously rotating director structure consisting of alternating bands of splay and bend deformation, as seen in Figs. 2(d) and 2(e). The formation of such a structure from a uniformly aligned nematic has never been observed, for two reasons. First, the flexoelectric effect must compete with ordinary dielectric anisotropy, and the latter coupling usually dominates, maintaining uniform orientation. Second, the continuously rotating director pattern would have to be formed by the generation and movement of defects through the sample, which would occur most easily with high static fields. However, high static fields usually induce electrohydrodynamic instabilities that would obscure the flexoelectric structure.

Starting from the helical cholesteric structure rather than the nematic ground state circumvents these two problems. The director is already continuously rotating in the cholesteric, in a pure twist fashion. It remains only for the flexoelectric effect to modify this structure to introduce components of splay and bend curvature. This is achieved by rotation of the director about an axis parallel to the electric field, as shown in Fig. 2. In both sign and magnitude the splay and bend deformations vary linearly with the rotation angle, at least at small angles. Our understanding of this geometry came partly from the elegant work of Bouligand, among others, who studied cholesteric structures in biological materials such as insect and crab cuticle and dinoflagellate chromosomes.[6] Microtomed specimens in which the slice is taken at an oblique angle to the cholesteric helix axis exhibit the multiply arched pattern of Figs. 2(d) and 2(e).

To make this model quantitative, consider a cholesteric helix in which the director $\hat{\mathbf{n}}$ is parallel to the x-y plane, with $n_x = \cos\theta$ and $n_y = \sin\theta$. In the presence of an electric field $\mathbf{E}$ along the x direction, it is proposed that the helix axis which was initially along the z direction rotates by an angle ϕ about the x axis (in the laboratory frame of reference, the helix axis is fixed for the sample geometry studied, and the x-y plane rotates by $-\phi$). Splay and bend deformations are described by vector fields $\mathbf{S}$ and $\mathbf{B}$, parallel to the x-y plane, given by $\mathbf{S} = \hat{\mathbf{n}}(\nabla\cdot\hat{\mathbf{n}})$ and $\mathbf{B} = \hat{\mathbf{n}}\times\nabla\times\hat{\mathbf{n}}$. Twist is described by $t = \hat{\mathbf{n}}\cdot\nabla\times\hat{\mathbf{n}}$. The free-energy density f for a cholesteric of equilibrium twist t_0 is

$$f = \tfrac{1}{2}\{K_1 S^2 + K_2(t_0 - t)^2 + K_3 B^2\} - e_s \mathbf{E}\cdot\mathbf{S} - e_b \mathbf{E}\cdot\mathbf{B} + (1/8\pi)\epsilon_a E^2 \sin^2\theta, \quad (1)$$

in which the K_i are the splay, twist, and bend elastic constants, e_s and e_b are the splay and bend flexoelectric coefficients, and ϵ_a is the anisotropic part of the dielectric constant.

To see the consequences of the flexoelectric effect in the simplest form, it is assumed that $K_1 = K_3$, $\epsilon_a = 0$, and $e_s = e_b = \bar{e}$, the mean flexoelectric coefficient. If we denote partial derivatives by subscripts, the free-energy

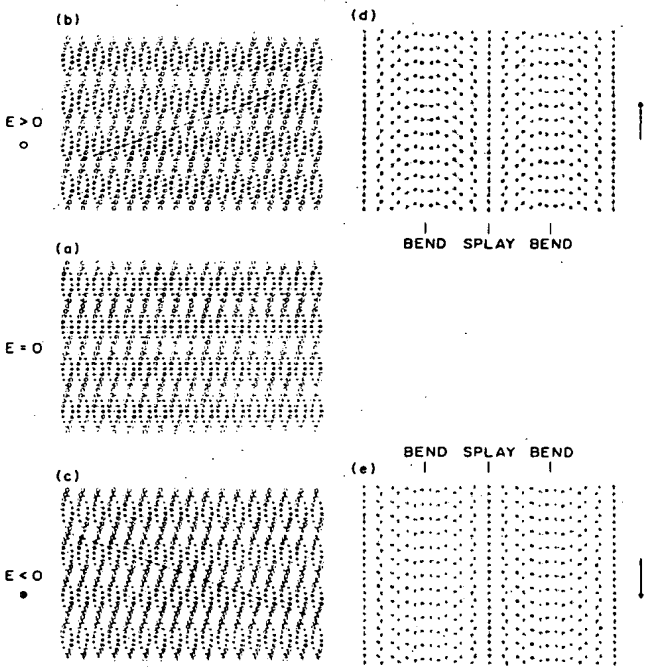

FIG. 2. The helical structure viewed normal to the helix axis, (a) in the absence of an electric field, and (b),(c) in the presence of an electric field perpendicular to the plane of the drawing, which shows the induced director rotation. (d),(e) Cross sections of the helix as indicated by the lines in (b) and (c), displaying the splay-bend pattern.

density reduces to

$$f = \tfrac{1}{2} K_1 \theta_y^2 - \bar{e} E \theta_y + \tfrac{1}{2} K_2 (t_0 - \theta_z)^2. \quad (2)$$

This is clearly minimized by $\theta_z = t_0$ and $\theta_y = \bar{e}E/K_1$. If we denote the rotated helix axis by a wave vector $\mathbf{k}$, with $\theta = \theta_0 + \mathbf{k}\cdot\mathbf{r}$, then $k\cos\phi = t_0$ and $k\sin\phi = \bar{e}E/K_1$. The rotation angle is given by $\tan\phi = \bar{e}E/t_0 K_1$, which is linear in E for small rotations. With use of this expression, and the value of the slope in Fig. 1, it is found that $\bar{e} = 3\times10^{-5}$ cgs units, for $K_1 = K_3 = 1\times10^{-6}$ dyn and helix pitch $= 0.5$ μm. This value is similar to those for other liquid crystals.[4,7] At first it may seem strange that the free energy is lowered by a uniform rotation of the molecules about the electric field direction, but it should be recalled that the flexoelectric coupling induces curvature, not alignment.

A drawback of this simplified theory is that it ignores the dielectric coupling, which distorts and eventually unwinds the helix. It is interesting to determine how the flexoelectric effect influences the helix unwinding field. Still, under the assumption of a uniformly rotated helix axis, the definition of a spatial coordinate h along the helix axis results in $\theta_z = \theta_h \cos\phi$ and $\theta_y = \theta_h \sin\phi$. Let us assume $K_1 = K_3$ to simplify the mathematics without serious loss of generality; then the free energy can be written

$$f = A\theta_h^2 + B\theta_h + C + \tfrac{1}{2} K_2 t_0^2, \quad (3)$$

$$A = \tfrac{1}{2}(K_1 \sin^2\phi + K_2 \cos^2\phi), \quad (4)$$

$$B = (-e_s \cos^2\theta - e_b \sin^2\theta) E \sin\phi - K_2 t_0 \cos\phi, \quad (5)$$

$$C = (1/8\pi)\epsilon_a E^2 \sin^2\theta. \quad (6)$$

This form of free-energy density can be dealt with by the same methods used to understand the unwinding of the helix by the simple dielectric coupling. The first integral of the Euler-Lagrange equation is given by $\theta_h = \pm[(C+Q)/A]^{1/2}$, in which Q is a constant of integration. θ can be written in terms of elliptic integrals. By our substituting this form of θ_h into the mean free energy and minimizing with respect to ϕ and Q, it is possible to derive expressions for the pitch of the helix and the rotation angle ϕ as a function of electric field. Surprisingly, the simple result for $\tan\phi$, derived above, remains valid even in this much more general case.

The critical field E_c for unwinding the helix is, however, modified by the flexoelectric coupling:

$$E_c = \tfrac{1}{2}\pi t_0 [4\pi K_2/(\epsilon_a - \pi^3 \bar{e}^2 K_1^{-1})]^{1/2}. \quad (7)$$

The effective dielectric anisotropy is thus reduced by the flexoelectric effect. Since the flexoelectric coupling tends to keep the director in a helical configuration, it opposes the dielectric coupling, and can substantially increase the critical field over what it would be if $\bar{e}$ were zero.

This prediction can be tested by the study of the frequency dependence of the flexoelectric effect and of the critical field. A remarkable feature of this form of the flexoelectric effect is that a small homogeneous rotation of all the molecules in the system produces a short wavelength periodic splay-bend structure with a small intrinsic relaxation time. In the materials that have been studied, the flexoelectric distortions follow the field up to frequencies of several kilohertz, above which rotational viscosity suppresses the response. At high frequencies therefore the critical field for unwinding the helix should decrease. In the materials that have been tested, the flexoelectric effect has been small enough and the frequency dependence of the dielectric anisotropy large enough to make this experiment ambiguous.

The practical applications of this new effect remain to be explored. To maximize the reponse, it is desirable to have a material which has large flexoelectric coefficients of the same sign, a requirement about which little is known at the level of designing new molecules. To achieve large rotation angles in this effect, it is necessary to avoid the unwinding of the helix by the dielectric coupling, which suggests that the dielectric anisotropy should be small. Eventually this effect may have application as a modulator of optical transmission or optical Bragg scattering.

We are very grateful to J. W. Goodby for stimulating discussions and for providing the liquid-crystalline materials.

[1]J. S. Patel, T. M. Leslie and J. W. Goodby, Ferroelectrics **59**, 129 (1984).
[2]N. V. Madhusudana and G. Durand, J. Phys. (Paris), Lett. **46**, L195 (1985).
[3]G. Durand, Mol. Cryst. Liq. Cryst. **113**, 237 (1984).
[4]J. Prost and P. S. Pershan, J. Appl. Phys. **47**, 2298 (1976).
[5]R. B. Meyer, Phys. Rev. Lett. **22**, 918 (1969).
[6]Y. Bouligand, J. Phys. (Paris), Colloq. **30**, C4-90 (1969).
[7]D. Schmidt, M. Shadt, and W. Helfrich, Z. Naturforsch. Teil A **27**, 277 (1972).

Submicrosecond bistable electro-optic switching in liquid crystals

Noel A. Clark [a] and Sven T. Lagerwall
Department of Physics, Chalmers Technical University, Goteborg, Sweden

(Received 3 March 1980; accepted for publication 13 March 1980)

Ferroelectric smectic *C* (FSC) liquid crystals are used in a simple new geometry that allows the spontaneous formation of either of two surface-stabilized smectic *C* monodomains of opposite ferroelectric polarization. These domains are separated by well-defined walls which may be manipulated with an applied electric field. The resulting electro-optic effects exhibit a unique combination of properties: microsecond to submicrosecond dynamics, threshold behavior, symmetric bistability, and a large electro-optic response.

PACS numbers: 61.30. – v, 78.20.Jq

In the smectic *C* (SC) liquid-crystalline phase molecules form a layered structure with the average orientation of the molecular long axes, denoted by the unit vector director $\hat{n}$ tilted at an angle Ω_0 to the layer normal ($\hat{z}$ axis). The director $\hat{n}$ exhibits a continuous degeneracy in its azimuthal orientation, lying on a cone coaxial with $\hat{z}$ (Fig. 1). The azimuthal orientation is thus readily manipulated by external forces or fields. Guided by an elegant physical argument, Meyer *et al.*[1] showed that, for suitably constructed chirally asymmetric molecules, the SC structue will be ferroelectric, with a macroscopic electric dipole density **P** locally normal to $\hat{n}$ and lying in the (x, y) plane of the layers. In principle, FSC's yield, as a result of **P**·**E** torques, a strong linear coupling of $\hat{n}$ to applied electric field **E**.[1,2] However, this linear coupling is eliminated on a macroscopic scale by an additional consequence of the molecular chirality, namely that $\hat{n}$ and **P** spiral about the $\hat{z}$ axis to form an effectively antiferroelectric helical structure. We demonstrate here that it is possible to use surface interactions to suppress the antiferroelectric helix in a geometry that simultaneously provides (i) the stabilization of either of two domains of opposite ferroelectric polarization separated by domain walls (a situation not permitted in the bulk because of the rotational degeneracy of $\hat{n}$); (ii) convenient **E** field selection of molecular orientation via domain-wall manipuation; (iii) a large optical response (equivalent to the rotation of a uniaxial dielectric of refractive index anisotropy $\Delta n \sim 0.2$ through an angle $2\Omega_0 \sim 45$.

Figure 1 illustrates the essential features of our geometry. The SC is confined between flat plates which are treated so that the director at a surface is constrained to lie in the plane of the surface ($\gamma_1 = 0$), but with no strong tendency for a particular orientation in the surface plane (γ_2 free). For samples having the layers normal to the plates, this boundary condition requires a disclinated texture in order to be

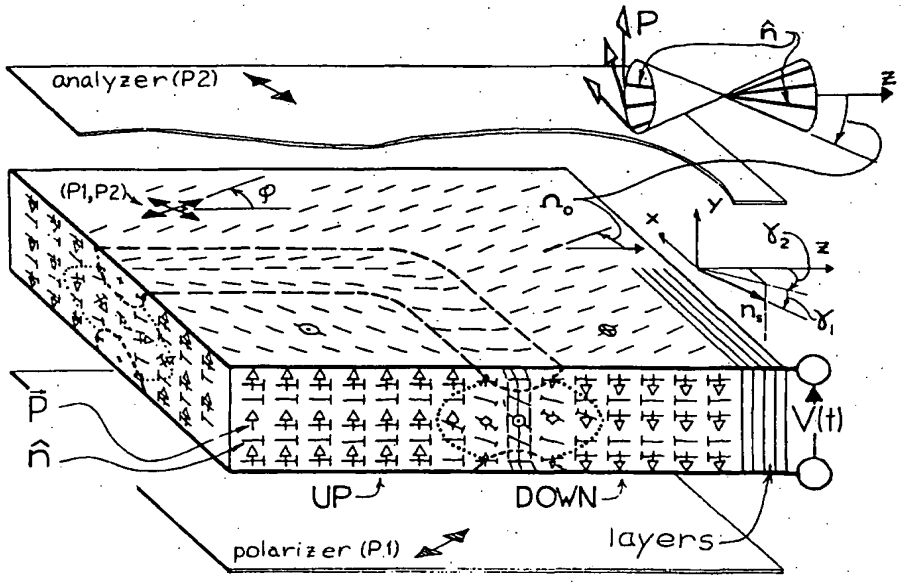

FIG. 1. Schematic of the sample geometry showing UP and DOWN domains and a domain wall (—| indicates a molecule whose right end projects outward). In the regions bounded by the dashed lines (-----) and the plates the SC tilt angle Ω is less than Ω_0. This represents the core of the disclination and, in fact, may be very small. There may also be small layer compression effects. The polarizer (P1) and analyzer (P2) are crossed, with the polarization direction at an angle φ to the $\hat{z}$ axis. For $\varphi = \Omega_0$, light traversing the polarizer-sample-analyzer sandwich will be extinguished in the DOWN state and transmitted in the UP state. A positive applied voltage moves the domain wall so that the DOWN region grows. Domain walls having the opposite helix sense are also possible and are observed.

[a] Permanent address: Dept. of Physics, Univ. of Colorado, Boulder, CO 80309.

 0003-6951/80/110899-03$00.50

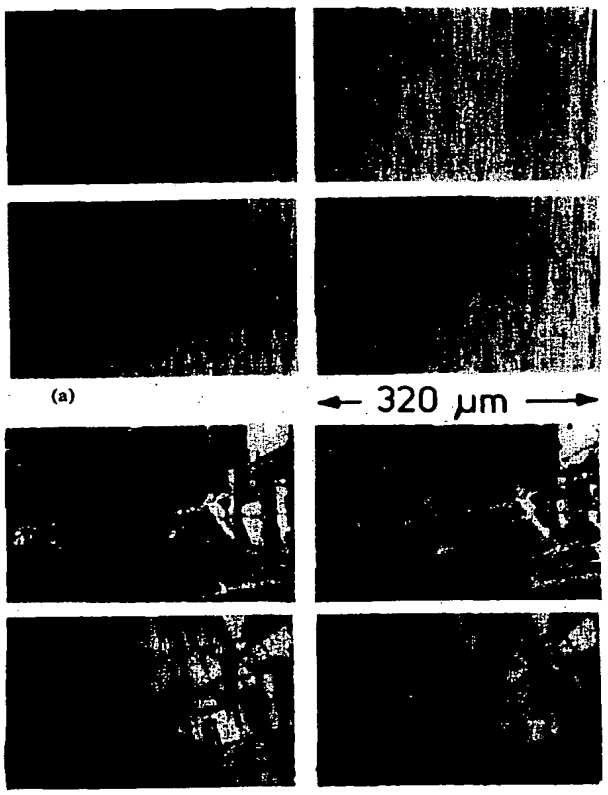

FIG. 2. Transmission micrographs (resolution $\sim 1\ \mu$m): (a) Domain-wall migration in a 1.5-thick SC DOBAMBC sample at $T = 84$ °C. The sample has been oriented by shear such that the layers are horizontal and normal to the page. The vertical texture is caused by remaining weak smectic layer undulations. The analyzer is horizontal and the polarizer is vertical making a small angle with the layer normal ($\varphi \cong 1°$). Voltage sequence (left to right and down): 0, 0.5, 1.0, 1.5 V. The transmitted light contrast between UP (bright) and DOWN (dark) domains is evident. This contrast reverses as the sample is rotated through $\varphi = 0$ and at $\varphi = 0$ only the domain walls are visible, dark, and sharp on a light background. Note the closed domain-wall loops, indicating the presence of domain walls of both signs, and the coalescence of two loops to make one. (b) Sample appearance with $\varphi = \Omega_0$ under conditions of bistable operation. Vertical texture is as in 2(a), and horizontal lines are thin homeotropic regions resulting from the orienting shear. These serve to nucleate and terminate domain-wall motion. Voltage sequence: 1, (top left) −5 V; 2, (top right) 0 V; 3, (bottom left) +5 V; 4, (bottom right) 0 V.

compatible with the bulk $\hat{n}$, P helix. Since the energy required to unwind the helix decreases as the sample thickness d, this boundary condition will suppress the $\hat{n}$, P helix[3] for sufficiently thin samples ($d \lesssim P$, the helix pitch). In the absence of the helix there are two stable, equal energy configurations of the SC, illustrated in Fig. 1 for the idealized case of complete freedom of angle γ_2. For FSC's these two types of $\hat{n}$, P monodomains will possess opposite P normal to the plates, and will be denoted as the "UP "and "DOWN" states. The UP and DOWN states are structurally identical, differing only by a π rotation about the $\hat{z}$ axis (symmetric bistability). Adjacent UP and DOWN regions in a sample will be separated by well-defined domain boundaries (Fig. 1) which are π inversion walls in the $\hat{n}$, P field. The application of a field favoring the UP orientation produces torques in the wall which induce wall motion that expands the UP region and vice versa. Possible structures for domain walls parallel and normal to the SC layers are shown in Fig. 1. Note that the domains in our case are stabilized by surface mechanical forces and not by bulk forces, distinguishing it from that of crystalline ferroelectrics.

The optical effects associated with domain-wall motion arise from the different director orientations in the UP and DOWN states. Although weakly biaxial,[4] the SC may be taken for present purposes to be uniaxial, with the optic (high index) axis along $\hat{n}$. The simplest geometry has the sample between crossed polarizers with $\hat{n}$ parallel to the polarization direction in the DOWN state ($\varphi = \Omega_0$, Fig. 1) leading to extinction of light passing through the polarizers and sample (DOWN = OFF). In the UP state the polarization will make an angle $2\Omega_0$ with the optic axis and a fraction of the incident optical power F will be transmitted, with

$$F = F_0[\sin(4\Omega_0)\sin(\pi \Delta n\, d/\lambda)]^2.$$

Here Δn is the refractive index anisotropy, λ the vacuum optical wavelength, and F_0 the parallel polarizer transmis-

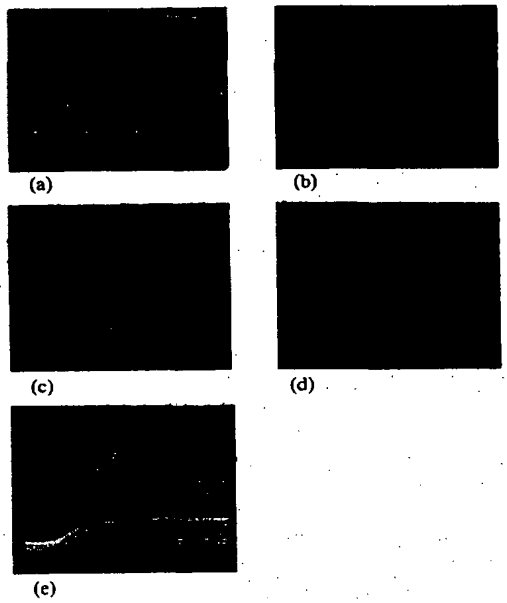

Fig. 3. Response of the optical transmission of a SC HOBACPC sample at $T = 68$ °C to pairs of opposite-polarity rectangular voltage pulses, spaced by 70 ms. VERT, photodiode output or applied voltage; HORIZ, time. (a) The top trace represents the optical response to above-threshold pulses showing switching to the OFF state at the beginning of the trace and back to the ON state 70 ms later. The ON pulses are above threshold for all traces. Top to bottom: response to OFF pulses of fixed width ($\tau = 1.4\ \mu$s) and variable amplitude $A = 44$, 37, 29, and 26 V (10 ms/div). (b) Photodiode response to OFF pulses of fixed amplitude ($A = 44$ V) and variable width: $\tau = 2.2$, 1.1, 0.9, and 0.6 μs (top to bottom), again the ON pulses are above threshold (10 ms/div). (c) Dynamic optical response showing applied pulse (top) and photodiode output (bottom): LEFT ($2\ \mu$s/div): $A = 20$ V, $\tau = 2.0\ \mu$s; RIGHT ($1\ \mu$s/div): $A = 40$ V, $\tau = 1.0\ \mu$s. (d) Dynamic optical response showing a series of b actinic pulses (top) of varying width for which $A = 1.5$ V and $20 < \tau < 240\ \mu$s, and photodiode response (bottom); 50 μs/div. Traces have been displaced vertically to avoid overlap. For $A = 1.5$ V full latching occurs for $\tau > 200\ \mu$s.

sion. $F = F_0$ can be achieved for $\Omega_0 \gtrsim 23°$ [this condition is met for DOBAMBC[5] for $T \lesssim 85$ °C (Refs. 2, 4)], and $d > \lambda/2\Delta n$, implying $d > 2.5\lambda \sim 1.2\,\mu$m ($\Delta n \sim 0.2$ for DOBAMBC[4]).

We now turn to our experimental results. The bounding plates were glass, coated with semitransparent conductive ($100\,\Omega/\text{cm}^2$) SnO_2 layers. The SnO_2 surfaces were cleaned of contaminants and dust with spectrographic acetone and placed together without spacers (overlap area = 6×6 mm). The sample material was introduced between them by capillary suction from the isotropic phase, resulting in samples which were slightly wedged, typically varying from 0.5 to 3 μm in thickness. The compounds used in this study were optically active DOBAMBC[5] and HOBACPC.[5] Observations of the SA textures obtained upon cooling from the isotropic and obtained as a result of a gentle shearing of the bounding plates suggest the operative boundary conditions for these compounds to be those described above ($\gamma_1 = 0, \gamma_2$ free). The overall behavior of the two compounds was qualitatively similar except as noted below.

In the SC phase the helix was absent and the electro-optic response was characterized by the motion of resolution-limited domain walls separating regions having apparent optic axes (as determined by the angle φ of the crossed polarizer-analyzer required for extinction) oriented at angles $\varphi \sim \pm\Omega_0$ from the layer normal. The domain walls thus separate regions of nearly opposite polarization. Contrast ratios were limited by the degree of layer orientation achieved, with 20:1 typical over millimeter square areas for $|\varphi| = \Omega_0$.

Figure 2(a) shows typical domain-wall appearance in the SC phase. With a slowly varying voltage the detailed motion of the domain walls was followed and indicated their strong interaction with defects in the layer structure, surface imperfections and scratches, and subresolution defects. this observation prompted a search for bistable operation, which was indeed found, as indicated by Fig. 2(b), showing a sample in either the UP or DOWN state for zero applied field. Bistability was further studied by applying pairs of opposite polarity rectangular voltage pulses of selectable amplitude A, width τ, and time separation to the sample. The sample transmission was monitored by passing a 2-mW He-Ne laser through the microscope to a photodiode. Figure 3 shows typical results obtained on a 1.5-μm-thick[6] HOBACPC sample at $T = 68$ °C for pairs of pulses separated by 70 ms. Figures 3(a) and 3(b) show respectively the optical response to pulses of fixed width ($\tau = 1.4\,\mu$s and varying amplitude, and to pulses of fixed amplitude ($A = 44$ V) and varying width. For $A\tau$ sufficiently large, the optical response is bistable, with the (+ , −) pulse latching the monitored area ($200 \times 200\,\mu$m) into the (ON, OFF) state. The bistable latching exhibits a relatively sharp threshold, going from zero to saturated memory response for a less than 25% change in $A\tau$. The dynamic behavior of the optical response to a pulse [c.f. Fig. 3(c)] is characterized by a rise time τ_r which depends on pulse amplitude, increasing from a minimum of 1 μs for $A = 20$ V to 4 ms at $A = 0.2$ V. In general, for latching to occur, A and τ must be such that the saturated optical response is achieved during the applied pulse. An exception to this occurs for short, high-voltage pulses ($A > 20$ V) for which, although the optical response time does not decrease below 0.9 μs, it does exhibit "inertia," continuing to saturation after termination of the pulse. This minimum response time is comparable to the RC time constant of the sample sandwich. Full switching could be achieved with pulse widths τ_l over the range $A = 55$ V, $\tau_l = 500$ ns ($A\tau_l = 25$ V μs) to $A = 0.2$ V, $\tau_l = 4$ ms ($A\tau_l = 800$ V μs). This general trend and fast response is expected from the simplest theoretical estimate: $A\tau_l \sim \eta d/P \sim 10^{-4}$ V s, where is an orientational viscosity, although the predicted $\tau_l \sim A^{-1}$ dependence is obeyed only at the higher voltages ($A > 10$ V). The full response, once attained, was stable over periods of at least several hours. The dynamic response to fast-rise-time pulses was homogeneous (i.e., independent of the size L of the sample area monitored for $L > 5\,\mu$m), reflecting the nucleation and motion of many domain walls. Results in DOBAMBC were similar, with rise times and requisite pulse widths two to three times longer, presumably a result of the smaller value of P in this material.[7]

To conclude, the effects described here are of potential use where electro-optic effects having fast response and/or built-in memory are required (for example, matrix-addressed video display). This work was supported by the Swedish Natural Science Research Council and the Swedish Board of Technical Development.

[1] R. B. Meyer, L. Liebert, L. Strzelecki, and P. Keller, J. Phys. Lett. 36, L69–71 (1975).
[2] P. Martinot-Lagarde, J. Phys. (Paris) 37-C3, 129–132 (1976).
[3] The suppression of the helix for the stronger boundary condition $\gamma_1 = 0$, $\gamma_2 = \Omega_0$ to form a unique stable SC monodomain has been demonstrated [M. Brunet and C. Williams, Ann. Phys. 3, 237–248 (1978)].
[4] S. Garoff, Ph.D. thesis, Harvard University, 1977 (unpublished).
[5] DOBAMBC is decyloxybenzylidene p'-amino 2 methyl butyl cinnamate. See Ref. 1; HOBACPC is hexyloxybenzylidene p'-amino 2 chloropropyl cinnamate. See P. Keller, S. Juge, L. Liebert, and L. Strzelecki, C. R. A. S. 282C, 639-641 (1976). Both compounds have isotropic-SA-SC-SF phases.
[6] Sample thickness was determined using the Newton color sequence.
[7] P. Martinot-Lagarde, J. Phys. (Paris) Lett. 38, L17-19 (1977).

An electro-optic device based on field-controlled anchoring of a nematic liquid crystal

P. Jägemalm,[a] L. Komitov, and G. Barbero[b]
Department of Microelectronics and Nanoscience, Chalmers University of Technology, 412 96 Göteborg, Sweden

(Received 30 December 1997; accepted for publication 21 July 1998)

A surface-controlled electro-optic device using a nematic liquid crystal enclosed between two thin spaced glass plates is presented. Modulation angles of the optic axis up to more than 70° can be achieved even for small applied voltages. The switching of the optic axis occurs with a large component in the plane of the sample even though the electric field is applied normal to the sample surfaces. The effect seems to be driven by the dielectric coupling of the liquid crystal molecules with the applied electric field. The field induced switching process is governed by the bounding surfaces that have been covered with obliquely evaporated SiO_x. The mechanism of the phenomenon is briefly discussed. © *1998 American Institute of Physics.* [S0003-6951(98)02238-4]

In nematic liquid crystals, the average orientation (**n**) of the long molecular axis of the rod-shaped molecules takes on the properties of a macroscopic optic axis. Since the orientation of the molecules is easily altered with external fields a number of electro-optic devices have been suggested and realized. One of the major applications for liquid crystals is in flat panel displays. Many of these displays have suffered from a limited viewing angle due to the fact that the switching of the molecules (and thus the optic axis) occurs perpendicular to the plane of the display area and the image contrast becomes dependent on the position of the observer. During the last 15 years attention has therefore been focused on techniques where the optic axis can be switched in the plane of the display.[1–3] However, for in-plane switching in nematics the electric field usually has to be applied in the plane of the display which causes problems with resolution and additional costs. One of the techniques suggested for avoiding this problem involves bistable switching of the liquid crystal molecules in a sandwiched cell whose substrates were covered with obliquely evaporated SiO_x.[4,5] In this letter we report on an electro-optic device where the switching is based on the same type of substrates.

Recently a temperature induced anchoring transition in nematic liquid crystals aligned by evaporated SiO_x has been reported.[6,7] It was shown that the molecular orientation in the so-called twofold degenerate alignment is temperature dependent. This type of alignment can be found for a small interval of evaporation angles,[6,8–11] typically in the range of 67°–75°. For higher and lower evaporation angles two uniform monostable types of alignment are found where the molecules lie in the evaporation plane (Σ) and with a certain pretilt ($\mathbf{n}\parallel\Sigma$, $0°<\theta<90°$, $\phi=0°$) for high evaporation angles and perpendicular to the evaporation plane and with zero pretilt ($\mathbf{n}\perp\Sigma$, $\theta=90°$, $\phi=90°$) for low evaporation angles, (see Fig. 1). Thus, the temperature induced anchoring transition mentioned above can be seen as a continuous transition between these two monostable states. Here, we report on how this anchoring transition is affected by applying an electric field perpendicular to the cell substrates, or in other words the electro-optic response of the cell in the transition region. The remarkable feature of our technique is that even though the field is applied perpendicularly to the cell there is an effective rotation of the optic axis in the plane of the sample. So far, the only similar study that has been performed in this field was presented by Nobili and Durand,[12] but it was performed for samples at the opposite limit of the twofold degenerate (bistable) alignment for another purpose.

The cells used in this study were of the conventional sandwich type consisting of two indium–tin–oxide (ITO) coated glass plates (Baltracon Z20) with alignment layers of obliquely evaporated SiO_x. The SiO_x was evaporated at 8 Å/s to a total thickness of 200 Å (measured perpendicular to the substrate) and at an angle $\alpha=74°$ from the substrate normal. All depositions were carried out at room temperature and in high vacuum (10^{-7} mbar, SiO source). Cells with cell gap $d=3$ and 6 μm were assembled. The nematic liquid crystal material used was E7 (Merck), which has positive

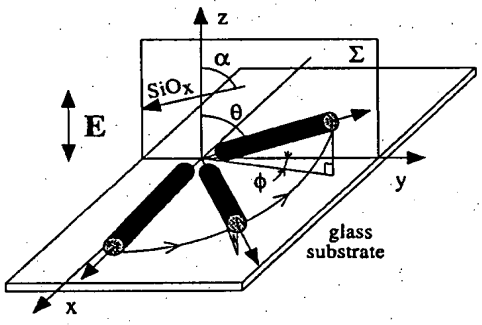

FIG. 1. Schematic representation of the switching of the liquid crystal molecules close to the interface cell substrate (SiO_x)/liquid crystal when an electric field is applied. The SiO_x evaporation plane is represented by Σ, the evaporation angle by α, and the polar and azimuthal angle by θ and ϕ, respectively.

[a]Electronic mail: jagemalm@fy.chalmers.se
[b]Present address: Dipartimento di Fisica and INFM, Politecnico di Torino, 10129 Torino, Italy.

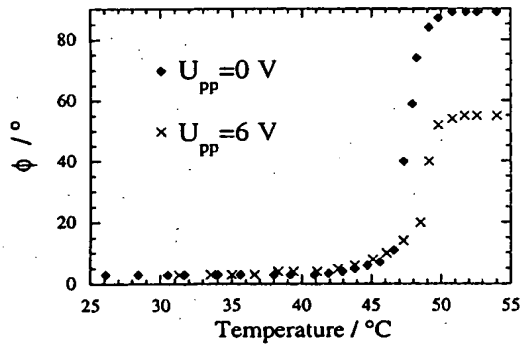

FIG. 2. The effect of an applied electric field (U_{pp}) on the temperature induced reorientation of the optic axis in a cell with the twofold degenerate alignment. Large switching angles can be achieved even for small applied voltages in the high temperature interval. The SiO_x evaporation angle is $\alpha = 74°$.

dielectric anisotropy, $\Delta\epsilon > 0$. The filling of the cells was performed under vacuum and with the liquid crystal material in the isotropic phase. Special attention was paid to the filling process since the selection of molecular orientation is strongly dependent on this process.[13] We were able to obtain textures with only one of the two possible orientations in the twofold degenerate alignment in most of the cells. The investigations of the cell textures were performed in a polarizing microscope (Zeiss Photo microscope II Pol.) equipped with a hot stage (Mettler FP52) for temperature control and with the possibility of applying ac or dc electric fields to the cells.

In a cell with the SiO_x alignment layer evaporated at $\alpha = 74°$ the director is found to be oriented close to the evaporation plane at low temperatures (see Fig. 2). As the temperature increases, the director reorients towards the position perpendicular to the evaporation plane with zero pretilt. (It has been shown that this anchoring transition essentially follows a plane which is tilted about 20° with respect to the substrate.[14] A small hysteresis has then been neglected.[6]) However, if an electric field is applied across the cell, the magnitude of the thermal reorientation of the preferred direction of alignment changes. The reorientation starts approximately at the same temperature independently of the applied voltage while the maximum rotation of the director is significantly smaller with the voltage applied than without (see Fig. 2). The higher the applied voltage is, the smaller the reorientation is. The voltage dependence depicted in Fig. 2 was obtained using an ac voltage of $f = 100$ Hz applied over the transparent ITO electrodes on the two substrates. By switching the electric field on and off, we can thus reorient the director and thereby achieve a large modulation of the azimuthal angle, ϕ, of the optic axis in the high temperature interval. Examples of such measurements are shown in Figs. 3(a) and 3(b) where the *normalized* azimuthal angle $\phi_{norm} = \phi_{max} - \phi(E)$ has been plotted for two cells with a different cell gap as a function of the applied voltage (ϕ_{max} is the maximum azimuthal angle induced by increasing the temperature, $\phi_{max} \approx 89°$). The maximum reorientation of the optic axis is found to be approximately 75°. However, at the high voltages required for these large angles the dielectric coupling with the electric field increases the average molecular tilt from the substrate and thus decreases the birefringence of the sample. The result is a decrease of the contrast. The optical response time is fairly short, about 1 ms in rise time (10→90%) and 1.5 ms in decay time for a pulse of 6 V applied to a cell with a cell gap $d = 6$ μm. The cell texture was homogeneous and the switching occurs over the entire electrode area.

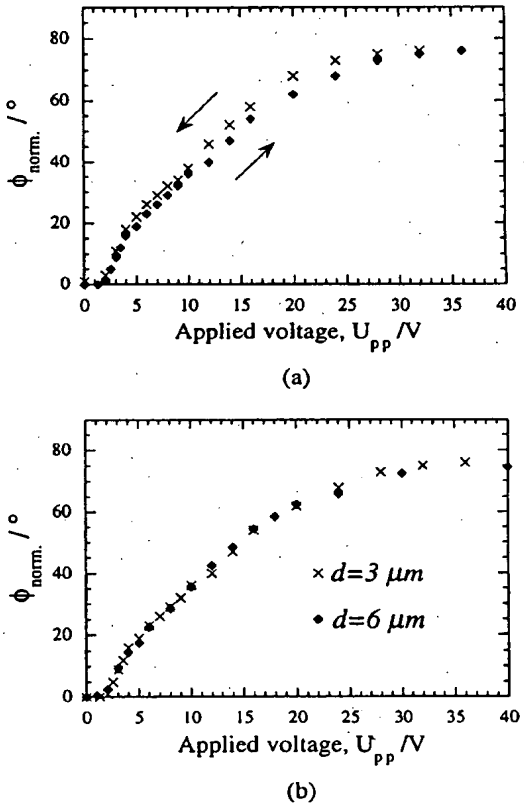

FIG. 3. Normalized azimuthal angle of the optic axis, ϕ_{norm}, as a function of the applied voltage (U_{pp} ac voltage, $f = 100$ Hz, $T \approx 50$ °C). In (a) (cell gap $d = 3$ μm) the small hysteresis found is shown, whereas in (b) a comparison between two cells with cell gap $d = 6$ μm and $d = 3$ μm is shown for increasing T. The evaporation angle is the same as in Fig. 2.

The reorientation of the optic axis shown in Figs. 3(a) and 3(b) has a small but noticeable threshold voltage. This is probably due to the symmetry of the initial nematic orientation and can be described as a Freedericksz transition effect.[15] The critical voltage for reorientation is then given by $V_c = E_c d = \pi\sqrt{k/|\epsilon_a|}$ [independent of cell thickness d, as shown in Fig. 3(b)] which for the nematic material E7 is on the order of 2 V. Above the threshold, the reorientation is almost linear for small applied voltages and then it saturates as the voltage is increased. To describe the effect of an applied electric field along the normal of the sample, $\mathbf{E} = E\mathbf{z}$, we write the total energy per unit surface area of the sample as[16]

$$F(\theta,\phi) = \int_{-d/2}^{d/2} \frac{1}{2} k \left\{ \theta'^2 + \sin^2\theta \phi'^2 \pm \frac{1}{\xi^2} \sin^2\theta \right\} dz + 2F_s(\theta_s, \phi_s), \quad (1)$$

where the sign + holds for positive dielectric anisotropy $\epsilon_a > 0$, and − for $\epsilon_a < 0$. The factor k is the nematic elastic constant (one constant approximation) and $F_s(\theta_s, \phi_s)$ is the

anisotropic part of the surface energy on the substrates at $z = \pm d/2\,[\theta_s = \theta(\pm d/2),\quad \phi_s = \phi(\pm d/2)]$. The term $\xi = \sqrt{k/(|\epsilon_a|E^2)}$ is the electric coherence length and gives an idea of the length over which the effect of the electric field on the director overcomes the orienting effects of the walls. Now, the actual values of $\theta(z)$ and $\phi(z)$ are the ones minimizing $F(\theta,\phi)$ given by Eq. (1). The minimization of Eq. (1) leads to differential equations with belonging boundary conditions. For voltages higher than the critical one, given by the Freedericksz transition described above, it is possible to show[17] that the contribution (F_{el}) from the applied electric field to the surface energy can be taken into account by changing the anisotropic part of the surface energy F_s to an "effective" surface anchoring energy, F_s^{eff}. To model the anisotropic part of the surface energy we make use of a Landau–de Gennes power series expansion which correctly describes the symmetry of the evaporated SiO_x surface.[14] The expansion has been shown to give a good fit of the temperature induced transition[14] where the director reorients on a plane, as described above. Let $p = \cos\theta_s$ and $q = \sin\theta_s \cos\phi_s$, then the surface energy can be expressed as

$$F_s^{\text{eff}}(\theta_s,\phi_s) = \tfrac{1}{2}Ap^2 + \tfrac{1}{4}Bp^4 + \tfrac{1}{2}aq^2 + \tfrac{1}{4}bq^4 + \tfrac{1}{2}cp^2q^2 + F_{\text{el}}, \tag{2}$$

where A, B, a, b, and c are temperature dependent phenomenological parameters. By minimizing the effective surface energy one deduces that[17]

$$(\nu + \eta\cos^2\theta_s)\cos\theta_s = \frac{V}{V_c}$$

and

$$\sin\phi_s = \frac{\sqrt{-[(a/b)+(c/b)\cos^2\theta_s]}}{\sin\theta_s}, \tag{3}$$

where ν, η and a, b, c are free parameters which can be used to fit experimental data and V is the applied voltage. Even though the model is simple and Eq. (3) above does not contain all the details of the reorientation (a more detailed description including simulations of experimental data is in progress[17]), it is evident that an induced change of the polar angle may also lead to a reorientation in the azimuthal direction. The qualitative idea is that the two angles θ and ϕ are coupled[8,6,14] and that the change of the polar angle θ, induced by the coupling with the field, automatically gives rise to a change in the azimuthal angle, at least for the molecules near the surfaces. This is supported by the fact that the model seems to give the most correct predictions when the molecules close to the surfaces are bound to reorient on an imaginary plane, which is characterized by the same parameters as previously used to described the plane for the temperature induced transition.

To conclude, we have presented a device based on an electro-optic effect that involves switching of the optic axis with a large component in the plane of the sample even though the electric field is applied normal to the bounding surfaces. Large switching angles can be achieved for small voltages and the optical response time is short (1 ms for $U_{pp} = 6$ V and $d = 6\ \mu$m). A simple model has been suggested, based on the dielectric coupling of the liquid crystal molecules with the applied electric field. If the temperature range of the twofold degenerate orientation can be extended, this new technique offers a wide potential for applications.

Two of the authors, P. J. and L. K., acknowledge financial support from the Swedish Research Council for Engineering Sciences. They also thank A. K. Zvezdin for fruitful discussions and I. Dierking for comments on the manuscript.

[1] N. A. Clark and S. T. Lagerwall, Appl. Phys. Lett. **36**, 899 (1980).
[2] R. Kiefer, B. Weber, F. Windsceid, and G. Baur, *Proceedings of the 12th International Display Research Conference* (Society for Information Display and the Institute of Television Engineers of Japan, Hiroshima, 1992), p. 547.
[3] M. Oh-e, M. Ohta, S. Aratani, and K. Kondo, *Proceedings of the 15th International Display Research Conference* (Society for Information Display and the Institute of Television Engineers of Japan, Hamamatsu, 1995), p. 557.
[4] R. Barberi and G. Durand, Appl. Phys. Lett. **58**, 2907 (1991).
[5] R. Barberi, M. Giocondo, and G. Durand, Appl. Phys. Lett. **60**, 1085 (1992).
[6] P. Jägemalm and L. Komitov, Liq. Cryst. **23**, 1 (1997).
[7] P. Jägemalm, D. S. Herman, L. Komitov, and F. Simoni, Liq. Cryst. **24**, 335 (1998).
[8] M. Monkade, M. Boix, and G. Durand, Europhys. Lett. **5**, 697 (1988).
[9] M. Monkade, These de Troisieme Cycle, Orsay, France, 1986.
[10] B. Jerome, Boix, and P. Pieranski, Europhys. Lett. **5**, 693 (1988).
[11] R. Barberi, M. Giocondo, M. Iovane, I. Dozov, and E. Polossat, Liq. Cryst. **25**, 23 (1998).
[12] M. Nobili and G. Durand, Europhys. Lett. **25**, 527 (1994).
[13] B. Jerome and P. Pieranski, J. Phys. (France) **49**, 1601 (1988).
[14] P. Jägemalm, G. Barbero, L. Komitov, and A. Strigazzi, Phys. Lett. A **235**, 621 (1997).
[15] V. Freedericksz and V. Zolina, Trans. Faraday Soc. **29**, 919 (1933).
[16] P. G. de Gennes, *The Physics of Liquid Crystals* (Clarendon, Oxford, 1974).
[17] P. Jägemalm, G. Barbero, L. Komitov, and A. K. Zvezdin (unpublished).